UNIVERSITY OF CALIFORNIA

Merced

Descriptive Analysis of the Turbulent Velocity Profiles for Two Cross Sections in a River Confluence Zone

A thesis submitted in partial satisfaction of the requirements for the degree Master of Science in Environmental Systems

by

Sandra Rocio Villamizar Amaya

2007

The thesis of Sandra Rocio Villamizar Amaya is approved

_____

Jeff Wright

_____

Carlos Coimbra

_____

Thomas Harmon, Committee Chair

University of California, Merced

2007

Table of Contents

List of Figures

List of Tables

ABSTRACT OF THE THESIS

Descriptive Analysis of the Turbulent Velocity Profiles for Two Cross Sections in a River Confluence Zone

by

Sandra Rocio Villamizar

Master of Science in Environmental Systems

University of California, Merced, 2007

Professor Thomas Harmon, Chair

Increasing demands on water supplies, along with concerns about non-point source pollution, and water quality-based ecological factors all point to the need for observing stream flow perturbations and pollutant discharges at higher resolution than has been practical until now. This work presents a rapidly deployable Networked Infomechanical System (NIMS RD) technology for observing spatiotemporal variability in hydraulic and chemical properties across stream channels. NIMS RD is comprised of two supporting towers and a suspension cable delivering power and Internet connectivity for controlling and actuating the tram-like NIMS unit. The NIMS unit is capable of raising and lowering

a payload of sensors, allowing a preprogrammed or data-actuated adaptive scan to be completed across a stream channel. This work examines velocity vectors in a real river system using an acoustic Doppler velocimeter (ADV) sensor with positioning controlled by the NIMS RD apparatus. Raster scans providing velocity fields for river cross-sections at the San Joaquin River-Merced River confluence are presented for low flow conditions in August of 2006 and 2007. Sensor dwell time is examined in an effort to determine optimal sampling rates for balancing experimental efficiency with the precision of observations. The observed velocity profiles are compared to theoretical vertical and transverse velocity profiles. While some aspects of the real and theoretical profiles agreed qualitatively, the real system exhibited more complicated behavior than the simplistic approach was capable of describing.

Descriptive analysis of the turbulent velocity profiles for two cross sections in a river confluence zone

1 Introduction

The development of stationary and mobile networked sensing technology is enabling more detailed investigation of river hydraulics than has been previously possible. Many theoretical postulations have been published related to transport and mixing in rivers. However, most of them are based on laboratory experiments for ideal cases and few have been tested in real environments. This thesis focuses on the observation and analysis of velocity distributions at the confluence of the San Joaquin and Merced Rivers, a site of ongoing experiments using a recently developed mobile, robotic sensor deployment platform.

The thesis is organized as follows. Chapter 2 presents motivation for developing methods for high-resolution river characterization. This is followed by a description of the experimental field site that is the subject of this thesis and the unique methods for acquiring the high-resolution data sets (Chapter 3). Chapter 4 presents the results and interpretation of the field efforts, the first portion of which pertains to the velocity fields and profiles observed in the confluence zone during low flow periods in 2006 and 2007. These velocity fields are compared with theoretical velocity distributions in order to validate this method for characterizing complex stream flow and mixing conditions. The major contributions of the thesis are outlined in Chapter 5 in the form of conclusions, which are expected to be applicable to major river confluences throughout the world.

2 Background

2.1 Salinity and Mixing on the San Joaquin River

Salinity is a critical problem in the San Joaquin River that is caused by the combination of upstream impoundments and the impaired quality of return flows from agricultural drainage, managed wetlands, groundwater inputs, and other distributed sources. There have been extensive efforts aimed at the improvement of San Joaquin River water quality and an understanding of the sources of its degradation (Brown, Panshin, Kratzer, Zamora, & Gronberg, 2004; Dubrovsky, Kratzer, Brown, Gronberg, & Burow, 1998; Gronberg et al., 1998; Kratzer & Shelton, 1998). These efforts have resulted in the development of water resources management tools (e.g., CALSIM II), which decision-makers use to balance water rights and other allocations with environmental flows on specific parts of the San Joaquin River. Most of these models (such as CALSIM II) are simple routing or one-dimensional advection-dispersion models, which assume uniform cross-sectional mixing in the river network (Department of Water Resources, Bay-Delta Office, 2002). However, as the demand for improved environmental quality increases, more sophisticated river models are be needed to evaluate flow fields and water quality distributions in complex mixing zones in order to better assess salt assimilative capacity and sediment transport issues, and to plan and assess river restoration efforts.

2.2 The flow structure downstream a river confluence

Understanding the flow structure at a river confluence constitutes an interesting problem since the mixing layer that forms between the two confluent streams determines the exchange of pollutants and sediments between them, which in turn impacts all the biological and chemical processes happening downstream. This section provides a description of several representative river confluence studies. The primary focus here is on the experimental methods for collecting velocity data which is the major emphasis of this thesis work.

An exemplary study by (De Serres, Roy, Biron, & Best, 1999) at the confluence of the Bayonne and Berthier Rivers in Canada used an array of four two-component Marsh McBirney Electromagnetic Current Meters (ECMs) to measure the structure of the three-dimensional flow between the confluence point to 26.5 m downstream. The velocity measurements start at 0.04 m above the bed with an average vertical spacing of 0.08 m and a sampling period of 60 seconds. The distribution of the sampling points was designed to maximize the downstream and lateral extent of the surveyed zone during a time period short enough to avoid significant changes in flow stage. Five cross sections were completed within the study reach with five or six velocity profiles taken along each section.

This 21-day study spanned different flow conditions associated with momentum flux ratios varying from 0.18 to 2.02 (ratio of momentum flux between the tributary and the main stream $Mr = \rho_{tributary} \cdot U_{tributary} \cdot Q_{tributary} / \rho_{main} \cdot U_{main} \cdot Q_{main}$), identified key characteristics for the confluence. First, the results confirmed the presence of a stagnation zone (zone of reduced velocities) at the apex of the junction with reversed flows in one of the confluent channels depending on the momentum flux ratio, and low velocities and no evident recirculation motion in the zone of the downstream junction. Second, the work identified a mixing zone characterized by a small decrease in mean velocities, an average streamline orientation towards the water surface and an increase in turbulent kinetic energy and in the turbulence intensity (i.e., a decrease in the mean velocity in the upstream portion of the confluence, corresponding to the highest levels of turbulent kinetic energy within the mixing layer due to turbulent eddies' extraction of energy from the mean flow). Third, the work demonstrated the effect of the momentum flux ratio on the positioning of the mixing layer and its effect on bed morphology and sediment transport (since the spatial distribution of the rates of bedload transport and associated morphological changes are controlled by the position of the mixing zone (Boyer, 1996)). Finally, the results illustrated the influence of bed discordance on the distortion of the mixing layer and the enhancement of fluid and momentum exchange and sediment dispersal between the two streams.

In another recent confluence investigation, (Sukhodolov & Rhoads, 2001) examined the three-dimensional structure of turbulence within the shear layer and within the ambient flow outside the shear layer, at three stream confluences with concordant beds, all located in Central Illinois. Acoustic Doppler Velocimeters (ADV) at sampling frequencies of 25 Hz were used. The results from this work confirmed the formation of a zone of stagnation flow near the junction apex, proposed by (Best, 1987) and observed by (De Serres et al., 1999). (Sukhodolov & Rhoads, 2001) defined the shear layer as a relatively narrow vertical band of highly turbulent kinetic energy which, for the case of concordant beds, remained vertical and did not exhibit lateral distortion or tilting. Also, this study found that beyond the stagnation zone, the shear layer and mixing interface coincided and were delimited by the mean flow of each of the two streams. However, further downstream, although the shear layer dissipated (it could not be identified in terms of turbulence data), the mixing interface persisted. Because of this, the authors suggested that turbulent diffusion within the shear layer was not highly effective at mixing the two confluent flows. Furthermore, they confirmed that turbulence within the shear-layer flow can be characterized as quasi-two-dimensional since, due to the depth-limited environment and bottom friction influence, the fluid motion is restricted in the vertical direction but not in the down-stream and cross-stream directions when looking at the large scale turbulent structures.

The two-dimensional character of the shear layer was confirmed by (Booij & Tukker, 2001) which proposed a simple model to predict the development of mixing layers in shallow flows (channel width >> channel depth). The velocity difference between the two confluent streams gives rise to instabilities in the fluid motion resulting in the development of the mixing layer. This work found that besides suppressing the large-scale structures (reducing the growth of the mixing layer), the bottom friction reduces the velocity difference across the mixing layer (transverse velocity difference) leading to a decrease in the mixing layer's spreading rate, which in turn affects the position of the center of the mixing layer towards the side of the slow ambient stream (by conservation

of mass, the decelerating fast ambient stream widens and the accelerating slow ambient stream narrows).

Most recently, (Rhoads & Sukhodolov, 2004) examined the confluence of the Kaskasia River and Copper Slough in East Central Illinois, recording the spatial and temporal characteristics of turbulence and coherent turbulent structures within a shear layer by using two three-dimensional ADVs (one fixed and the other mobile). Among the findings of this study was that coherent structures could be identified through cross-correlation analysis of the velocity time-series for different measurement locations. For the case of the analysis of the stream-wise velocity (u), maximum correlations decreased relatively slowly over short separation distances but decreased rapidly for separation distances greater than about 2 times the flow depth. Correlations were greatest for the stream-wise and transverse velocity components and weakest for the vertical velocity component. Also, a comparison between convective, local and spatially averaged velocities found that convective velocities of coherent structures derived from the correlation analysis differed from local mean velocities and from spatially averaged mean velocities, indicating that coherent structures evolved as they were transported along the shear layer. Finally, a domain of quasi-two-dimensional turbulence energy at low frequencies was found to be associated with large-scale intrusions of fluid from one stream into the other along the mixing interface.

The previous studies have presented important characteristics of river confluences such us the presence of a stagnation zone (zone of reduced velocities) at the junction's apex followed by a mixing zone for which development is dependent on the velocity difference, and bed friction and the bed concordance/discordance condition (defining the position, lateral distortion and tilting of the shear layer). Also, the two-dimensional character of the large-scale (low-frequency) turbulent structures at the shear layer is confirmed. All of these hydrodynamic features are based on the analysis of the distributed velocity data collected.

In the previous references velocity sampling times from 60 seconds up to 600 seconds were used in order to characterize the large turbulent structures at the mixing layer. (De Serres et al., 1999) used a sampling period of 60 seconds arguing that it was sufficient to include the major structures of the flow. (Sukhodolov & Rhoads, 2001) and (Rhoads & Sukhodolov, 2004) used a minimum sampling time of 300 seconds after doing an analysis of variance which concluded that the record length was sufficient to capture major sources of variation in velocity. Finally, (Booij & Tukker, 2001) used a 600-second averaging time for each sampling point. Although they did not present justification for the use of this sampling rate, it can be attributed to the fact that their data was taken in a dedicated shallow water flume.

3 San Joaquin-Merced River confluence experimental site

3.1 Site description

The confluence between the San Joaquin and Merced rivers is located between the Merced and Stanislaus counties at 37º20'57" N and 120º58'30" W, with an elevation of 17.4 m (57 ft) above sea level (Figure 3-1). The study site covers an area including the two confluent rivers 100 m upstream, and the San Joaquin River 290 m downstream of the confluence point. While both rivers are impounded, the Merced River is currently managed on a schedule which provides greater environmental flows than the San Joaquin, and it arrives at the confluence relatively cleaner and colder. With the exception of relatively wet periods, the incoming San Joaquin River flow is mainly a combination of agricultural drainage and groundwater seepage by the time it reaches the confluence. Recent legal rulings have mandated that environmental flows be restored to the San Joaquin River via the Friant Dam above Fresno beginning in Fall 2009. Hence, the dynamics of the San Joaquin confluence with the Merced (and with other tributaries) is expected to change in the near future.

An interesting feature from the figure is the confirmation of the development of the shear layer which, due to velocity, water quality, and/or geomorphologic differences between the two rivers, extends for many channel widths downstream of the confluence point, in accord with the findings of (Biron, Ramamurthy, & Han, 2004; Booij & Tukker, 2001; Rhoads & Sukhodolov, 2004).

Figure 3-1. Geographical location of the confluence area (Source Google Earth – modified by the author)

3.2 Confluence characterization effort

Since 2005, the confluence of the San Joaquin and Merced Rivers has been the test bed for the evaluation of the Rapidly Deployable Networked Info-Mechanical System (NIMS RD), a robotic system designed for the collection of high-resolution information (distributed flow and water quality parameters) in river cross sections. NIMS RD results are intended to help improve our understanding of both small and large-scale phenomena including flow structure, contaminant fate and transport, and groundwater-surface water interactions. This document focuses on the 2006 and 2007 efforts.

During the period from August 22 - 25, 2006, NIMS RD was erected as a platform for deploying velocity and water quality sensors in two transects across the Merced and San Joaquin Rivers confluence. The objective of the experiment was to obtain a better understanding of the flow structure and mixing within the confluence zone. The sensors deployed at the two cross sections measured water quality parameters such us temperature, specific conductivity, pH, among others (by using a multiparameter probe), and flow field (by Acoustic Doppler Velocimeter - ADV). This experiment yielded a high resolution data set of coupled velocities and water quality parameters for the transect (denominated Transect 2), located 135 meters downstream of the confluence point. Results from the first transect (denominated Transect 1) were incomplete due to a data communication error.

A more ambitious study was undertaken at the same site during August 6-12, 2007. NIMS RD was deployed across four different cross sections, two located downstream of the confluence point, and the other two located upstream at each of the two confluent rivers. During this experiment the transect designated Transect 1, located 290 m downstream of the confluence point, was continually sampled and yielded 10 high resolution velocity data sets.

As an initial reference, velocity and water quality data for the two rivers for the times of the experiments are summarized in Table 3-1. The parameters were obtained from the California Department of Water Resources through its CDEC website (California Department of Water Resources, 2007).

Table 3-1. Basic flow and water quality data during the NIMS RD deployments (Source: California Digital Exchange Center, CDEC).

Date	Transect / Run	Time span	Station	Mean Stream Flow (m^3/s)	Mean Temperature (deg C)	Mean Specific Conductivity (µS/cm)
08/25/2006	2	11:07:32 to 14:12:32	FFB	8.34	25.05	840.00
			MST	24.75	20.78	68.80
			NEW	31.13	--	--
08/07/07	1 / 1	12:03:17 to 14:09:42	FFB	3.89	24.54	1078.00
			MST	6.01	24.00	214.00
			NEW	11.91	--	--
	1 / 2	14:19:13 to 15:29:03	FFB	3.91	25.77	1065.00
			MST	5.61	25.41	220.33
			NEW	12.03	--	--
	1 / 4	18:13:03 to 18:36:22	FFB	3.91	26.76	1020.00
			MST	4.94	26.50	230.50
			NEW	11.96	--	--
	1 / 5	18:48:26 to 19:56:08	FFB	3.91	26.56	1020.00
			MST	4.66	26.11	235.50
			NEW	11.87	--	--
08/09/07	1 / 17	12:22:46 to 14:29:36	FFB	4.13	25.51	1043.00
			MST	3.65	24.15	330.75
			NEW	11.25	--	--
08/10/07	1 / 26	17:20:26 to 19:27:20	FFB	3.31	28.47	1158.00
			MST	4.16	28.11	308.33
			NEW	9.71	--	--
08/11/07	1 / 27	10:37:51 to 12:41:43	FFB	3.28	24.97	1188.00
			MST	4.12	23.11	298.33
			NEW	9.62	--	--

Verification of the flow data for the times of each NIMS RD run is necessary to determine whether stationary or transient conditions exist during sampling windows.

3.2.1 NIMS RD components description

NIMS RD is a technology created by the Center for Embedded Networked Sensing (CENS)* that introduces a new form of infrastructure-supported mobility enabling sensor nodes to explore and characterize complex three-dimensional environments (Harmon et

* http://research.cens.ucla.edu/portal

al., 2007). There are two main components to the system. The physical infrastructure is comprised of two fixed structures located at each side of the channel transect to support a static cable over which a tram-like NIMS unit is transported. Two independent motor and cabling systems permit the horizontal movement of the NIMS unit, and vertical movement of the sensor payload which is suspended from the NIMS unit. All the activity executed by the tram-like NIMS unit is controlled through the software component of the system consisting of a series of algorithms developed to allow continuous and autonomous control of node (i.e., sampling) position. NIMS RD may be preprogrammed for raster or adaptive scans across the stream channel. A more complete description of the system is provided by (Singh et al., 2007). The sketch in Figure 3-2 depicts the layout and functionality of the NIMS RD system.

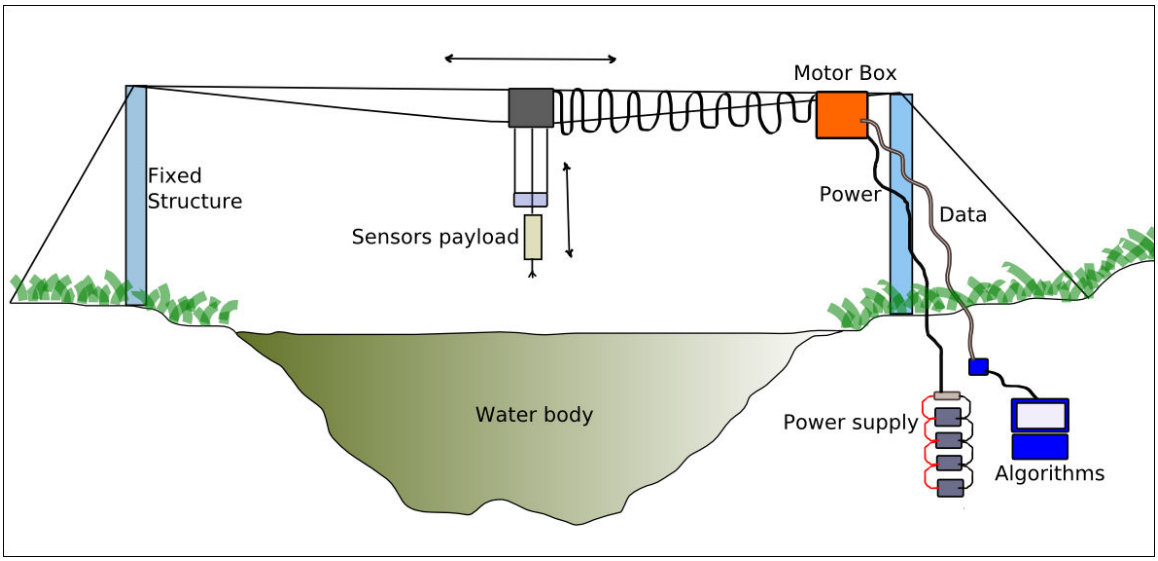

Figure 3-2. Schematic of the NIMS RD system

Deploying NIMS-RD at a river transect requires the following steps. First, the set up of the physical infrastructure with all its components (fixed structures, static, calibration, horizontal and vertical cables; motor box, tram unit, power sources, and communication system), followed by the horizontal calibration of the system (the spatial definition of the transect done by vertically aligning the tram at specific horizontal distances e.g., y = 0, 10, 20 m, until covering the channel width, with the help of a marked calibration cable).

Once the calibration is completed, the definition of the cross section's profile for each particular transect is done during a process referred to as plumbing. This process is developed by lowering the node at each defined y position until reaching the river bottom. The values obtained can be compared against sonar measurements used to develop the bathymetry of the confluence area.

The spatial information collected during both calibration and plumbing allow defining a spatial grid within the cross section with discrete points at which the payload of sensors can be sent in order to sample the parameters of interest. The combination of grid granularity and sampling strategy (raster versus adaptive, sensor dwell times) is captured in the sampling design file and determines the overall duration of a scan.

3.3 The sampling process

Raster scans completed during the deployments and analyzed in this document are summarized in Table 3-2.

3.3.1 Transect 2 (2006)

On August 25, three-dimensional velocity components for Transect 2 were measured by using ADV (SonTek Argonaut ADV). A multiprobe Hydrolab DS5 was used to sample Temperature (T), pH, Specific Conductivity (SC), Turbidity, Luminescent Dissolved Oxygen (LDO), and Depth. The time for the experiment was 3 hours 5 minutes. The grid size was defined as every 1 m in the y (horizontal) direction, and every 0.6 m in the z (vertical) direction. The sampling strategy used was continuous sampling, averaging every 10 seconds with a total dwelling time of 30 seconds for each sampling point to yield three mean velocity values at each point. The photograph in Figure 3-3 shows the deployment of NIMS RD in Transect 2.

Table 3-2. NIMS RD deployment schedule (see section 3.4 for details on sensor equipment and measured parameters).

Date	Time	Transect / Run	Sensors	Data collected	Sampling Strategy
08/25/06	11:07:32 to 14:12:32	2	ADV Multi-parameter water quality sonde	3-D velocity vectors, T, pH, SC, Turbidity, LDO, Depth	Internal continuous sampling; 30-sec dwelling time; 10-sec average; 3 samples per point (293 points)
08/07/07	12:03:17 to 14:09:42	1 / 1	ADV Multi-parameter water quality sonde	3-D velocity vectors, T, pH, SC, Depth25, LDO, Chlorophyll	Real time continuous sampling; 60-sec dwelling time; 3-sec average; 20 samples per point (114 points)
	14:19:13 to 15:29:03	1 / 2			Real time continuous sampling; 30-sec dwelling time; 3-sec average; 10 samples per point (114 points)
	18:13:03 to 18:36:22	1 / 4	ADV	3-D velocity vectors	Real time continuous sampling; 300-sec dwelling time; 3-sec average; 100 samples per point (5 points)
	18:48:26 to 19:56:08	1 / 5			Real time continuous sampling; 300-sec dwelling time; 3-sec average; 100 samples per point (15 points)
08/09/07	12:22:46 to 14:29:36	1 / 17	ADV Multi-parameter water quality sonde	3-D velocity vectors, T, pH, SC, Depth25, LDO, Chlorophyll	Real time continuous sampling; 60-sec dwelling time; 3-sec average; 20 samples per point (114 points)
08/10/07	17:20:26 to 19:27:20	1 / 26			Real time continuous sampling; 60-sec dwelling time; 3-sec average; 20 samples per point (114 points)
08/11/07	10:37:51 to 12:41:43	1 / 27			Real time continuous sampling; 60-sec dwelling time; 3-sec average; 20 samples per point (114 points)

3.3.2 Transect 1 (2007)

From August 7 – 11, 2007, data for Transect 1 were obtained as described in Table 3-2. The main difference between the two experiments (2006 and 2007) is in the sampling strategies used. For Transect 1 in 2007, a real time continuous sampling strategy was used for the measurement of the three-dimensional velocity components. At a frequency of 10 Hz, the sensor internally averages every 3 seconds allowing to obtain for each sampling point 10 or 20 mean velocity values according to the dwelling time used in the raster (30 or 60 seconds, respectively). For all the raster samplings but two (runs 4 and 5), the velocity data can be associated to water quality parameters (T, pH, SC, Depth25, LDO, and Chlorophyll).

Transect 1 (2007) was located at the exact same position of the incomplete Transect 1 (2006), with the difference that for the flow conditions of 2007, the cross section presented a width of 40 m (10 m less than in the summer of 2006) and a maximum depth of 1.85 m (1.12 m less than in the summer of 2006). The grid size was defined as every 2 m in the y (horizontal) direction, and every 0.25 m in the z (vertical) direction. The photograph in Figure 3-4 shows the deployment of NIMS RD in Transect 1.

Figure 3-3. NIMS RD deployed in Transect 2 (2006) executed on the San Joaquin River just downstream of the Merced River confluence.

Figure 3-4. NIMS RD deployed in Transect 1 (2007)

3.4 Description of the sensors/loggers used during the experiment

3.4.1 Acoustic Doppler Velocimeter (ADV)

The acoustic Doppler velocimeter used, SonTek Argonaut ADV (Figure 3-5), is a single-point, 3-D Doppler current meter designed for shallow water monitoring (SonTek, 2007), with a 3-beam down-looking operation probe, a compass/tilt sensor providing the velocity data in East-North-Up (ENU) coordinate system (cm/s velocity units for the metric system), and auto-velocity range configuration within its measurement range (0.01 to 600 cm/s).

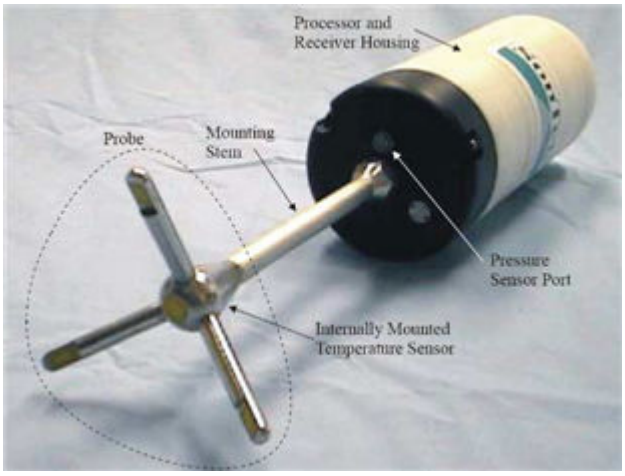

Figure 3-5. Sontek Argonaut-ADV (Source: Argonaut ADV Operation Manual, page 1)

The fact of having installed the compass/tilt sensor on the ADV represents an important advantage since the reported velocities account for the probe orientation (heading –angle between the probe x-axis and the north-), and its local rotations (pitch –rotation around the probe y-axis, and roll –rotation around the probe x-axis). See Figure 3-6. Argonaut ADV axes configuration and rotations.

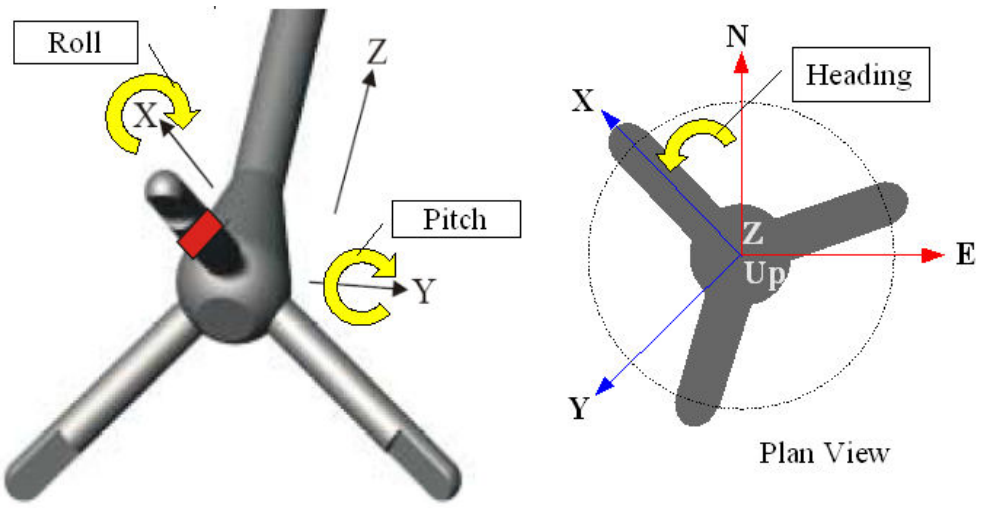

Figure 3-6. Sontek Argonaut-ADV axes configuration and rotations. Local rotations, pitch and roll (left), and probe oritentation, heading (rigth). (Source: Argonaut ADV Operation Manual, modified by the author)

Two different sampling strategies were used during the deployments offering some advantages and disadvantages in terms of the data analysis. In the internal continuous sampling strategy, the sensor averages velocity measurements or "pings" (10 pings per second) over the user-specified time and returns an averaged velocity value for each velocity component, each one accompanied by the corresponding standard error (giving an indication of the quality of the data). As the averaging interval is increased, the uncertainty in each sample is reduced (since the number of averaged pings is increased) as it is the internal instrument noise which, for the auto-velocity range configuration, can be ±1% of the measured velocity (for 1-second averaging interval), ±0.25% of the measured velocity (for 15-second averaging interval), and ±0.1% of the measured velocity (for 60-second averaging interval).

The disadvantage of this strategy is that since only one averaged velocity measurement is obtained for the specified time interval, it is not possible to develop any statistical analysis of the averaged velocities. Furthermore, the quality of the averaged velocity depends upon the duration of the averaging time.

The real time continuous sampling strategy allows the investigator to obtain one mean velocity value every three seconds (minimum averaging time allowed by the sensor), providing a number of mean velocity samples depending on the defined dwelling time, thus allowing to perform statistical analysis over the sampled velocities. The disadvantage of this strategy is related to the internal instrument noise which is bigger for small averaging times (~ ±1% of the measured velocity for 3-sec averaging time).

3.4.2 Multi-parameter water quality sonde

The water quality sonde used during the two experiments is Hydrolab DS5 (Figure 3-7). This multi-parameter probe, designed for in-situ and flow-through applications, is capable of reporting up to 15 measured and measured-derived parameters simultaneously(HACH Environmental,). Although various parameters were measured during the two experiments, a basic description is given here for temperature, pH, and specific conductivity.

Figure 3-7. Hydrolab DS5 multi-probe

3.4.2.1 Temperature

Temperature is important to chemical and biological processes occurring in a water body. Chemical species/compounds concentrations, animal and plant's aquatic life (reproduction, metabolism, growth) among others, are temperature-dependent

phenomena. The Temperature sensor used reports in a range of –5 to 50 °C with an accuracy of ± 0.10 °C, and a resolution of 0.01 °C.

3.4.2.2 pH

pH expresses the Hydrogen-ion concentration which indicates acidic or basic conditions. The Hydrolab pH electrode reports in a range from 0 to 14 units with an accuracy of ± 0.2 units, and resolution of 0.01 units.

3.4.2.3 Specific conductivity

Specific conductance correlates with the sum of dissolved major-ion concentrations in water and often with a single dissolved-ion concentration. The elements whose ionic forms contribute the most to these measures include: calcium (Ca2+), magnesium (Mg2+), sodium (Na+), potassium (K+), bicarbonate (HCO3-), sulfate (SO42-), and chloride (Cl-).

Specific conductance refers to measurements of conductivity that are made at or corrected to the standard temperature of 25ºC, taking into account that conductivity is the ability to conduct an electrical current when dealing with electrolytic or ionic conduction. Conductivity is reported in units μSiemen/cm (μS/cm) (Miller, Bradford, & Peters, 1988). The Specific Conductance sensor reports in a range of 0 to 100 mS/cm ($1x10^5$ μS/cm) with an accuracy of ± 1% of reading (± 0.001 mS/cm), and a resolution of 0.0001 units.

Specific conductance is used to calculate the total dissolved solids (TDS) concentration (mg/L) in the water which is a measure of water pollution. TDS accounts for the organic and inorganic substances contained in the water that pass trough a 2 μm sieve. TDS can be estimated by multiplying the specific conductance by a factor that varies between 0.55 and 0.9, depending on the soluble components of the water and on the temperature of the measurement. Relatively high factors may be required for saline or boiler waters, and lower factors may apply where considerable hydroxide or free acid is present (APHA, 1999).

4 Results and discussion

The analysis of the velocity distributions both in the vertical and transverse directions constitutes an interesting problem from the hydraulics point of view because most of the research regarding this problem has been done under laboratory conditions. Here, we examine the data collected at the San Joaquin River confluence, a natural channel with non-uniform flow and irregular cross sections, relative to theoretical profiles for well-defined channels. Although it was not expected that the San Joaquin data would agree closely with theoretical profiles, it was anticipated that there would be sufficient agreement to inform future sampling designs.

4.1 Vertical velocity distribution in turbulent flows

The velocity distribution in turbulent non-uniform flows has been found to be described by the law of the wall in the inner region of the velocity profile where the viscous (molecular) shear dominates, and by the velocity-defect law in the outer region of the velocity profile where the turbulent (eddy) shear dominates. An overlap layer exists where both types of shear are important and a profile smoothly connects the inner and outer regions (Kironoto & Graf, 1995; Nezu & Nakagawa, 1993; White, 2006). (Tachie & Bergstrom, 2000) presents the schematic of the typical velocity profile in an open channel (see Figure 4-1).

The inner region has been found to depend upon wall shear stress (τ_w), fluid properties (ρ), and distance from the wall (z) but not upon free stream parameters (Prandtl, 1933). Thus, after dimensional analysis:

$$\frac{u}{u_*} = f\left(\frac{z\,u_*}{\nu}\right), \qquad \textbf{(4-1)}$$

where $u_* = \sqrt{\tau_w / \rho}$ is the wall-friction velocity and ν is the kinematic viscosity of water.

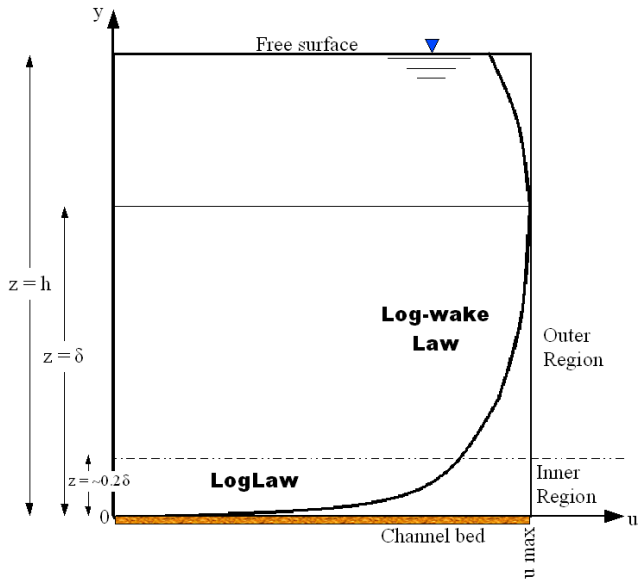

Figure 4-1. Schematic of the typical velocity profile in an open channel (Source: Tachie et. al., 2000, modified by the author)

In the outer region, the wall acts as a source of retardation reducing the local velocity $\bar{u}(z)$ below the freestream velocity (U_∞) in a manner independent of viscosity (μ) but dependent upon wall shear stress (τ_w), layer thickness (δ), and free stream pressure gradient (dp/dx) (White, 2006). After dimensional analysis:

$$\frac{U_\infty - \bar{u}}{u_*} = g\left(\frac{z}{\delta}, \xi\right), \tag{4-2}$$

where, $\xi = (\delta/\tau_w)(dp/dx)$ is local pressure gradient. Equation 4-2 is called the velocity-defect law because $\left(U_\infty - \bar{u}\right)$ represents the defect or retardation of the flow due to wall effects.

Lastly, the overlap layer is said to be the region where the inner and outer functions merge together $(\bar{u}_{inner} = \bar{u}_{outer})$. Then, for a particular pressure gradient ξ value:

$$\frac{\bar{u}}{u_*} = f\left(\frac{\delta\, u_*}{\nu}\frac{z}{\delta}\right) = \frac{U_\infty}{u_*} - g\left(\frac{z}{\delta}\right),$$

For the inner variables: $$\frac{\bar{u}}{u_*} = \frac{1}{\kappa}\ln\frac{z u_*}{\nu} + B \qquad \textbf{(4-3)}$$

For the outer variables: $$\frac{U_\infty - \bar{u}}{u_*} = -\frac{1}{\kappa}\ln\frac{z}{\delta} + A$$

where, $\kappa \approx 0.41$ and $B \approx 5.0$ are near-universal constants for turbulent flow past smooth, impermeable walls and A varies with the pressure gradient ξ (White, 2006).

4.1.1 The law of the wall

The law of the wall is typically applied in the zone of the velocity profile where $(z/\delta) < 0.2$, being z the elevation from the reference level to the mean velocity point of interest and δ, the thickness of the boundary layer. In this region the characteristic scales of length and velocity are ν/u_* (viscous length scale) and u_* (wall-friction velocity) respectively, allowing the definition of the dimensionless variables

$u^+ = \dfrac{\bar{u}}{u_*}$ (the normalized velocity), and

(4-4)

$z^+ = \dfrac{z}{(\nu/u_*)} = \dfrac{z\, u_*}{\nu}$ (the normalized length).

Three different sections can be identified in this zone: the viscous sublayer which extends from the no slip at the wall to $z^+ \le 5$ presenting a linear velocity profile, the buffer layer from $5 \le z^+ \le 30$ where the velocity profile is a smooth merge between the linear of the

viscous sublayer and the logarithmic profile, which extends until $z^+ \le 100-300$. For the fully developed turbulent region, the law of the wall is expressed as:

$$\frac{u}{u_*} = \frac{1}{\kappa}\ln\left(z^+\right) + B \quad , \tag{4-5}$$

where

u is the mean point velocity at a distance z measured from the reference level z_o,

κ is the von Karman constant (0.41),

B is a constant of integration (5.0).

4.1.2 The velocity-defect law

Difficulties in fitting the velocity profile of the outer region ($z/\delta > 0.2$) in a universal curve (due to the dependency of the outer region velocity on the pressure gradient) were overcome by Coles in 1956, who noticed that the deviations of the outer layer velocity above the log-law had a wake-like shape when viewed from the freestream. He found that if normalized by the maximum deviation at $z = \delta$, the data nearly collapse into a unique function of z/δ:

$$\frac{u^+ - u^+_{\log-law}}{U^+_\infty - u^+_{\log-law}(z=\delta)} \approx f(\frac{z}{\delta}) \quad , \tag{4-6}$$

where the wake function f is normalized to be zero at the wall and unity at $z = \delta$. If $\eta = z/\delta$ then, for $z = 0 \to \eta = 0$ and for $z = \delta \to \eta = 1$, two popular curve fits are used for the S-shape expected for the function:

$$f(\eta) \approx \sin^2\left(\frac{\pi}{2}\eta\right) \quad or \quad f(\eta) \approx 3\eta^2 - 2\eta^3 \quad . \tag{4-7}$$

By adding the wake to the log-law, it is possible to have an accurate approximation of both the overlap and outer layers:

$$u^+ = \frac{u}{u_*} \approx \frac{1}{\kappa}\ln(z^+) + B + \frac{2\Pi}{\kappa} f\left(\frac{z}{\delta}\right) \quad \textbf{(4-8)}$$

Equation 4-8 represents satisfactorily any two-dimensional turbulent-boundary-layer profile. $f(z/\delta) = \frac{2\Pi}{\kappa}\sin^2\left(\frac{\pi z}{2\delta}\right)$ is Cole's wake function and Π is Cole's wake strength parameter which accounts for the deviation from the law of the wall. This law applies over the entire depth such that in the wall region the Cole's wake function can be neglected ($\Pi = 0$), returning to the original law of the wall.

The velocity-defect law, valid for the entire depth of the velocity profile has the following form:

$$u_{\max}{}^+ - u^+ = \frac{u_{\max}}{u_*} - \frac{u}{u_*} = -\frac{1}{\kappa}\ln\left(\frac{z}{\delta}\right) + \frac{2\Pi}{\kappa}\cos^2\left(\frac{\pi z}{2\delta}\right) \quad \textbf{(4-9)}$$

The value of $\prod$ has been found to depend on the Reynolds number such that for values of $R_* = \delta u_* / \nu$ less than 500, $\prod$ is about zero; for small values (but bigger than 500), $\prod$ increases rapidly with R_*; and for values greater than 2000, $\prod$ remains nearly constant ($\prod \approx 0.2$) (Nezu & Nakagawa, 1993). Figure 4-2 presents the theoretical curve for the wake law. As it can be seen, at z/δ= 0.2, the data deviates from the law of the wall which applies only for the inner region of the velocity profile.

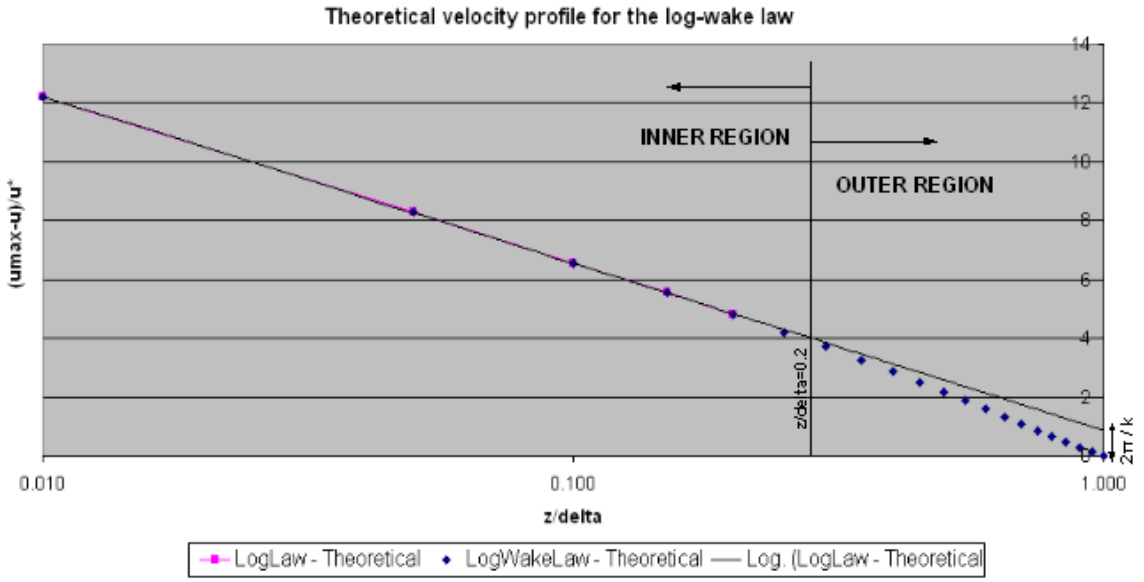

Figure 4-2. Theoretical velocity profile for the log-wake law (Source: (Kironoto & Graf, 1995)**. Modified by the author).**

4.2 Transverse velocity distribution in a turbulent mixing layer

The transition zone between contiguous flows with different velocities intensifies the lateral exchange of material and momentum and so is of importance for the dispersion of pollutants and sediment. The velocity difference between the two confluent streams generates a velocity shear which gives rise to Kelvin-Helmholtz instabilities in the fluid motion resulting in the development of the mixing layer. For natural confluences, these can be modeled by using depth-averaged shallow-water models, since the flows are confined between the bottom and the free surface thus restricting their mean flow and large-scale turbulent motions to mainly the horizontal plane.

(Booij & Tukker, 2001) proposed an integral method applied over the shallow-water equations to predict the development of the mixing layer in the longitudinal direction. Figure 4-3 presents the theoretical transverse velocity profile of the confined shallow mixing layer with the following considerations:

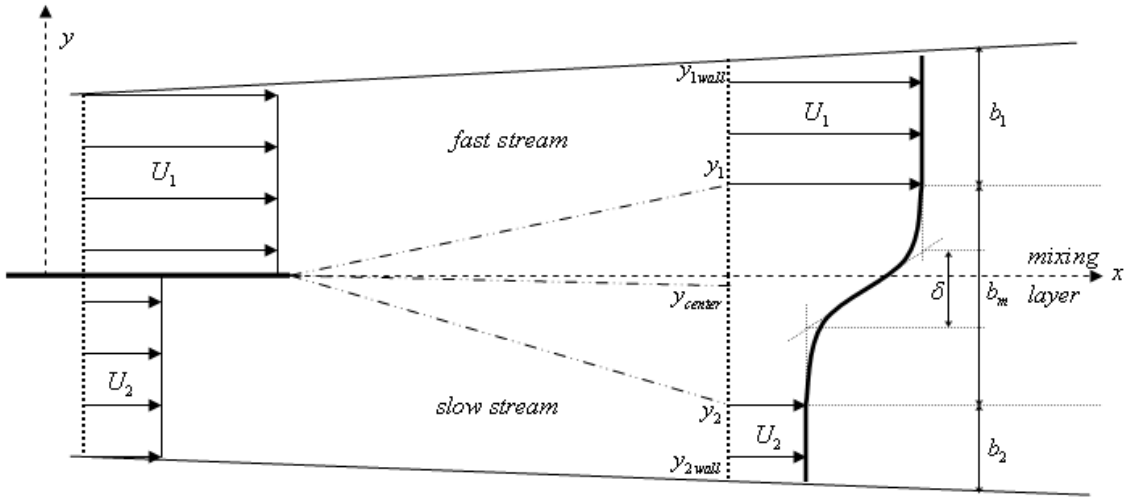

Figure 4-3. Scheme of a laterally confined shallow mixing layer (source (Booij & Tukker, 2001)**, modified by the author).**

1. The ambient fast stream is located within $(y_1 \le y < y_{1w}) = b_1$, the mixing layer region within $(y_2 < y < y_1) = b_m$, and the ambient slow stream within $(y_{2w} < y \le y_2) = b_2$.

2. There is no flow across the side-walls $(V_{y1w}, V_{y2w} = 0)$, and the influences of the boundary layers along the side-walls are neglected $(T_{xy} = 0)$.

3. The flow conditions at the internal boundaries y_1 and y_2 can be approximated with the flow conditions of the ambient streams. At $y = y_1$, $U = U_1$ and $T_{xy} = 0$. At $y = y_2$, $U = U_2$ and $T_{xy} = 0$. This is accomplished as long as y_1 and y_2 are located far from the mixing layer center. For this to happen, the width of the mixing layer region $b_m = y_1 - y_2 = \beta\delta$ has to be defined such that β is large enough to include the layer with considerable shear and small enough to remain between the sidewalls, leaving ample room for the ambient streams. An important condition of this model is that the sidewalls are far enough from the mixing layer so that there is no influence of them in the development of the mixing layer.

4. For the ambient streams the transverse profiles of the longitudinal velocity U are assumed to be uniform: $U = U_1$ for the fast stream, and $U = U_2$ for the slow stream.

5. For a cross section, the free surface level (z_f), the bottom channel level (z_b) and hence the depth h are considered to be constant. This assumption is made on the basis that the transverse slope of the free surface can be neglected when compared to the longitudinal slope.

6. For all the analyses, uniform bottom friction coefficient c_f and uniform slope of the river bed $(i = dz_b / dx)$ are considered.

The downstream evolution of a free mixing layer is described by (Booij & Tukker, 2001) in terms of the evolution of the width of the layer (δ) defined as the maximum-slope thickness of the mean velocity profile. The $\delta(x)$ gives an indication of the local scale of the flow:

$$\delta \equiv \frac{\Delta_U}{\left(\partial u/\partial y\right)\max} \text{ where, } \Delta_U = U_1 - U_2 . \qquad \textbf{(4-10)}$$

The development of the mixing layer is controlled by the bottom friction in two forms: the suppression of the development of the large-scale structures, and the reduction of the velocity difference between the two confluent streams. For the former, (Booij & Tukker, 2001) differentiates three different zones according to its development: first, the near field, located downstream of the junction of the two streams, in which the flow develops as a free mixing layer since in this section the width of the layer is smaller than the water depth and the influence of the bottom on the mixing layer is small. However, the bottom turbulence present in the ambient streams can stimulate a slightly higher initial spreading rate $(d\delta / dx)$. In the second zone, the middle field, the bottom friction influences strongly the development of the mixing layer by reducing its spreading rate. Finally, in

the far field, the stabilizing influence of the bottom friction suppresses the generation of new large-scale eddies, leading to near zero-growth of the mixing layer.

For the latter, recalling that the shear stress at the wall is dependent on the depth-averaged velocity squared, and the definition of the bottom-friction coefficient $(c_f = \tau_{wall} / (1/2\ \rho U^2))$, the bottom shear stress working on the fast stream is larger than the one on the slow stream, consequently generating more bottom friction on the earlier. In order to comply with the conservation of mass principle, the velocity of the fast stream is decelerated (and its cross sectional area increased) producing a decrease of the cross sectional area of the slow stream (and the increase of its mean velocity). This situation results in the reduction of the transverse velocity difference across the mixing layer which in turn leads to a decrease of the spreading rate. As the conservation of mass principle is satisfied, the center of the mixing layer formed between the two streams suffers a shift towards the accelerating stream.

Figure 4-4 presents the computed development of the mixing layer in river confluences for 5 different cases by (Booij & Tukker, 2001), with case 1 being the actual field data, cases 2 and 3 high velocity differences between the confluent rivers, and cases 4 and 5 similar velocities to the field data but with variations in the width ratio between the confluent rivers. Parameters such bed slope, bed friction coefficient and channel depth are considered constant for all the cases.

Noticing that bed discordancy, secondary flows, angle at the junction between the two confluent channels, among others, are factors not considered in the model, the findings of this reference are summarized as short development lengths and small widths of the mixing layer excepting the cases with very large velocity differences between the confluent rivers where the biggest mixing layer widths and development lengths are predicted.

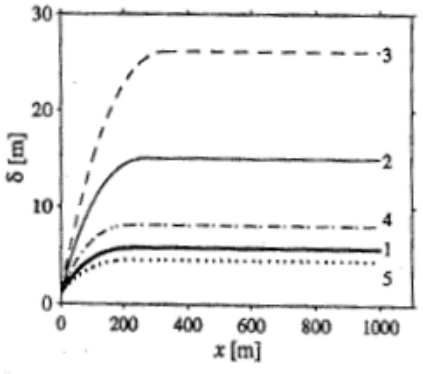

Case	U_1(m/s)	U_2(m/s)	b_1(m)	b_2(m)
1	1.4	0.8	100	200
2	2.0	0.5	100	200
3	2.5	0.25	100	200
4	1.4	0.6	150	150
5	1.4	0.92	50	250

Figure 4-4. Computed development of the mixing layer in river confluences (source (Booij & Tukker, 2001)**).**

4.3 Analysis of Transect 2 (2006)

4.3.1 General flow description

Transect 2 has a cross sectional area (A) of 131.94 m^2, a maximum water depth (D) of 4.3 m, a width (b) of 72 m, an aspect ratio ($\alpha = b/D$) of 16.7, an average temperature (T) of 22.3 ^oC. The cross section averaged-velocity magnitude (U) is 0.23 m/s. The previous characteristics allow calculating the dimensionless Reynolds and Froude numbers, which permit the description of the flow regime (the former) and the influence of gravity on fluid motion (the latter).

The value obtained for the Reynolds number confirms the turbulent regime of the flow at the evaluated cross section indicating that the inertial forces are stronger than the viscous forces.

$$\mathrm{Re}_x = \frac{Inertial\ forces}{Viscous\ forces} = \frac{\rho UL}{\mu} = \frac{UL}{\nu} = \frac{(0.23m/s)(2.58m)}{9.48X10^{-7}m^2/s} = 6.26X10^5, \quad \textbf{(4-11)}$$

where,

U is the mean fluid velocity (*m/s*) = 0.23,

L is the characteristic length (*m*) = 2.58. The characteristic length is the height at which velocity is maximum. An assumption of *L=0.6 (maximum depth)* is done due to the variability of the location of maximum velocities and depths across this natural river cross section, then $L = 0.6 * 4.3 = 2.58m$.

ρ is the fluid density (Kg/m^3).

μ is the dynamic fluid viscosity ($Pa \cdot s$ *or* $Kg/m \cdot s$)

ν is the kinematic viscosity ($\nu = \mu / \rho$ in m^2/s)

$$\nu = \frac{\mu}{\rho} = \left[1.14 - 0.031(T-15) + 0.00068(T-15)^2\right] X\ 10^{-6}\ m^2/s \quad \text{†} \qquad \textbf{(4-12)}$$

$$\nu = \left[1.14 - 0.031(22.3-15) + 0.00068(22.3-15)^2\right] X\ 10^{-6}\ m^2/s$$

$$\nu = 9.49 X 10^{-7} m^2/s.$$

For the Froude number, the calculated value indicates that the state of the flow is subcritical (Fr < 1). Consequently, the gravity forces are dominant over the inertial forces.

$$Fr = \frac{Inertial\ forces}{Gravity\ forces} = \frac{U}{\sqrt{gL}} = \frac{0.23m/s}{\sqrt{(9.8m/s^2)(4.3m)}} = 0.035 \qquad \textbf{(4-13)}$$

where,

U is the mean fluid velocity (*m/s*) = 0.23,

---

† Julien, Pierre Y. Erosion and Sedimentation.

g is the acceleration of gravity (m/s^2) = 9.8,

L is the characteristic length (m) = 4.3 A wide open channel (b >> D) can be assumed as a rectangular channel, for which the characteristic length L is the hydraulic depth *H*. For rectangular channels, it is equal to the depth of the flow section.

The flow at the cross section can be defined as subcritical-turbulent which is the case for many lowland rivers.

4.3.2 Descriptive analysis of the velocity profile

Transect 2 (2006) can be classified as a wide channel since the aspect ratio α is bigger than the critical value ($\alpha_c \approx 5$). For this particular case, the strength of the secondary currents due to sidewall effects can be reduced within the central region of the cross section of width $b - \alpha_c D$ (Nezu & Rodi, 1985) in (Gonzalez, Merching, & Oberg, 1996). The analysis of the velocity profile is done from $y = 20\,m$ to $y = 50\,m$ $(0.29 \le y^* \le 0.68)$, spanwise, thus avoiding sidewall effects, and providing four or more sampling depths for each vertical profile.

The first step in the in the analysis of the velocity data collected with the ADV for Transect 2 (2006) is the transformation of the velocity components from ENU system to the xyz-cross section system. Figure 4-5 (left) illustrates how the transformation is made. Two points with known (GPS) coordinates located within the cross-section alignment permit referencing the transect data within the ENU coordinate system. Each of the east (E) and north (N) velocity components can be transformed to the corresponding x and y component by using the adequated trigonometric function. Figure 4-5 (right) presents the new xyz coordinate system.

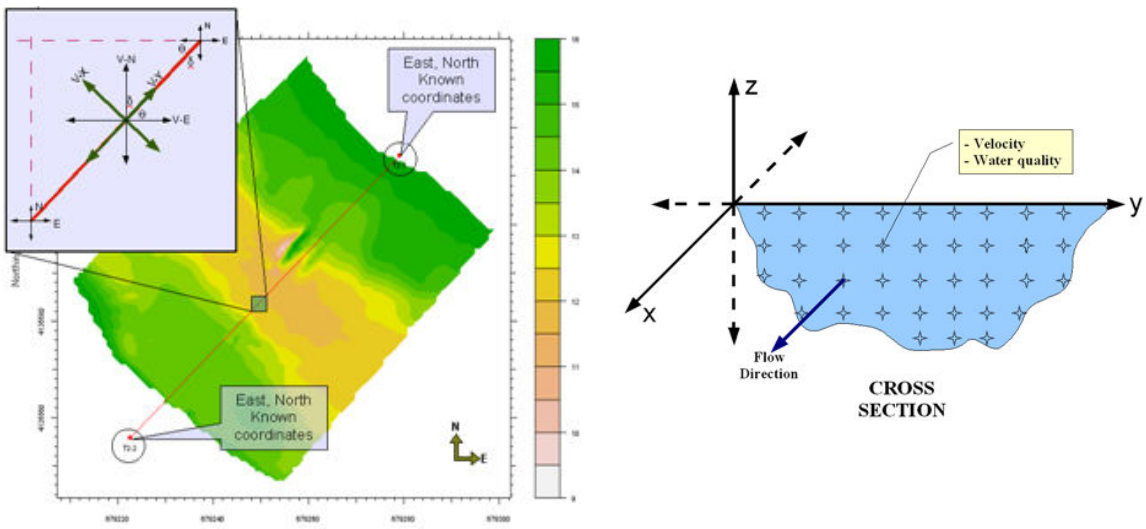

Figure 4-5. Left: Coordinates transformation schematic. Right: New XYZ coordinate system.

By normalizing the depth of each vertical profile, it is possible to plot the components of the velocity (vx, vy, and vz) along the normalized depth (from 0 to 1). In Figure 4-6 (top), vx represents the longitudinal component, vy the transverse component, vz the vertical component, and vxyz.Mag, the total velocity magnitude. As expected, the vertical component, vz, is not dominant (values tend to be close to zero), while transverse, vy, and longitudinal, vx, have strong components. Inspection of vxyz.Mag (total velocity magnitude) data allows the identification of outliers, considered as values lying outside the typical range presented in the dataset (vxyz.Mag ranging from 0.006 to 0.058 m/s) and characterized by large standard errors. Eleven velocities fall outside the typical range, and all of them correspond to measurements made close to the river bed ($z / h = 0.06$ *to* 0.13). Furthermore, all of these points have a common characteristic being that their standard errors have the greatest reported value (0.255 m/s).

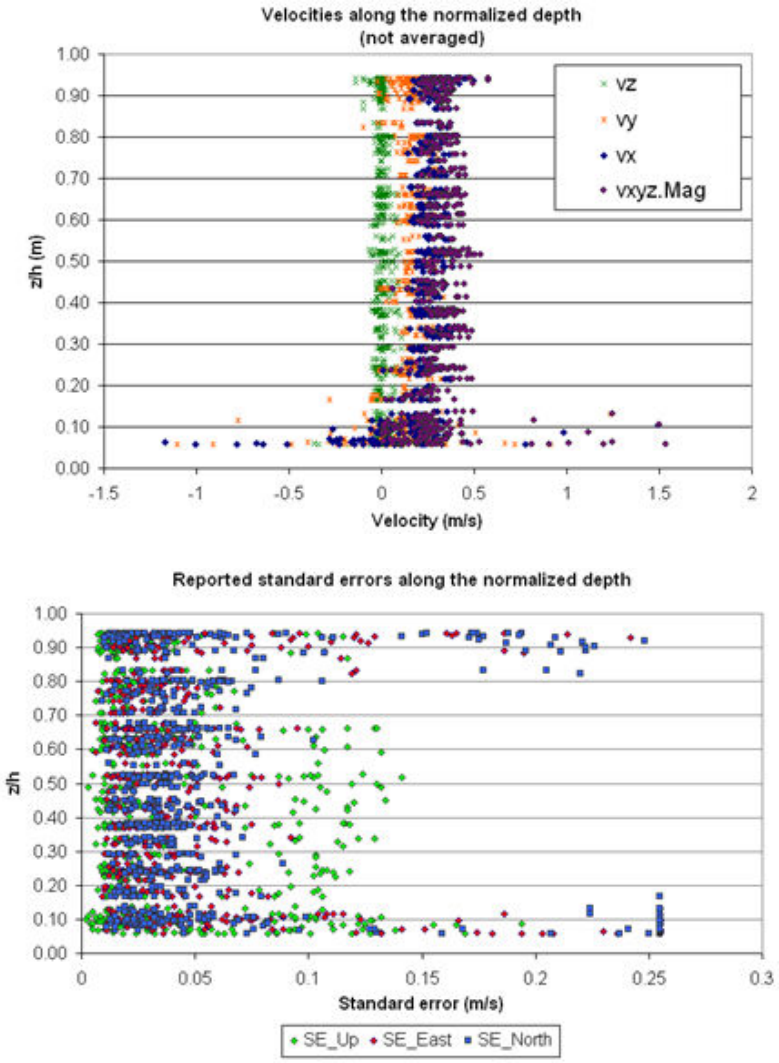

Figure 4-6. Top: Velocity values along the normalized depth. Bottom: Reported standard errors for the East and North velocity components, along the normalized depth.

Following the analysis of the standard errors reported by the sensor, a plot of the reported standard errors (SE) with respect to the normalized depth, Figure 4-6 (bottom), helps to define a threshold. Since the important components for the velocity analysis are the longitudinal and transverse, velocity values that report standard errors greater than 0.15 m/s in the east and north components, are considered to be faulty data. Ninety two (92) out of the 637 values (including the eleven mentioned above) fall in this range. Figure 4-7 presents the filtered data set of the transformed velocities and sensor reported standard errors.

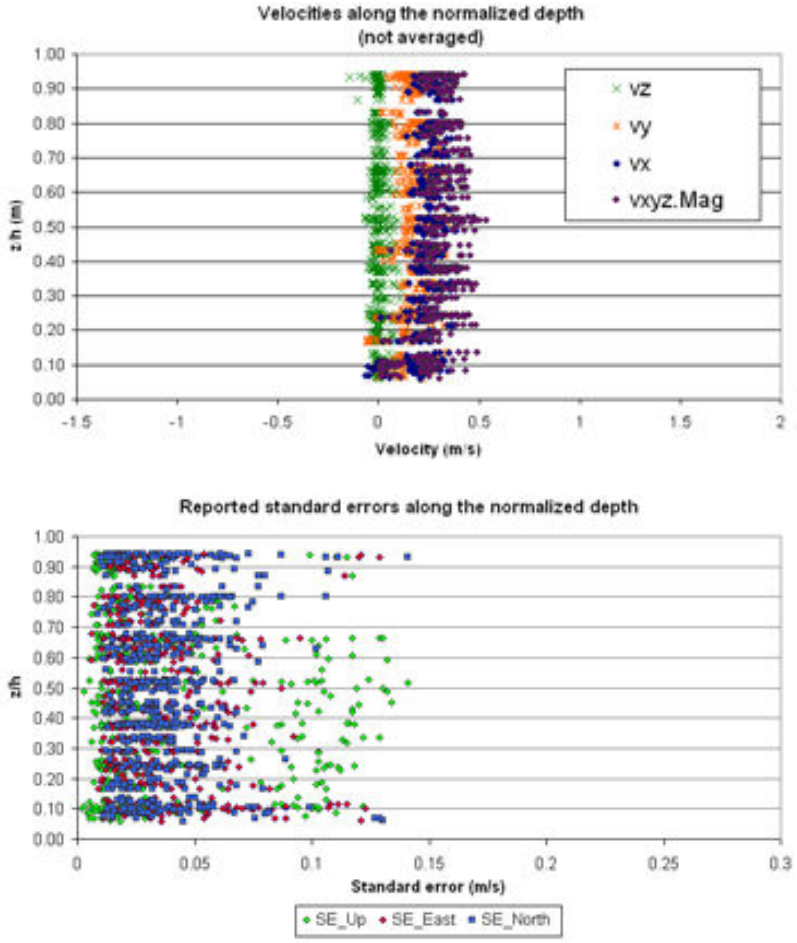

Figure 4-7. Velocities (top) and standard errors (bottom) along the normalized depth after data filtering.

Once the filtering process is accomplished, a t-test for the 95% confidence level is applied to the mean sampling velocities at each sampling point. These data sets are used in the velocity profile analysis. For the transect under study, from the spanwise distance $y = 20\,m$ to $y = 50\,m$ $(0.29 \le y^* \le 0.68)$, 15 vertical profiles are selected to analyze the mean velocity distribution. Figure 4-8 presents the distribution of the normalized velocity $(v^* = vxyz / v_o,\ v_o = 0.55\,m/s)$ along the normalized depth $(z^* = z/h)$. The value $v_o = 0.55\,m/s$ is chosen since the maximum value of mean velocity for the velocity profiles is $0.53\,m/s$.

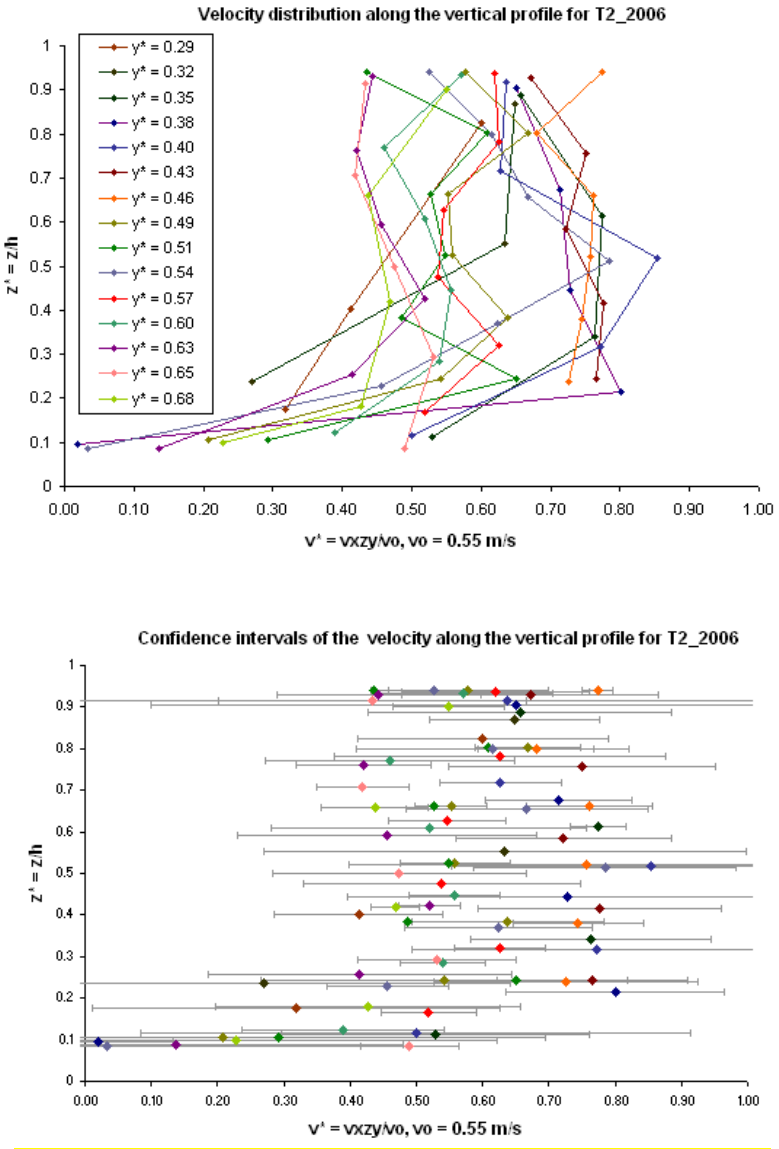

Figure 4-8. Normalized vertical velocity profile in Transect 2 (top). Confidence intervals for the vertical velocity profile (bottom).

In the figure, the confidence intervals of the mean velocities indicate high variability throughout the vertical dimension, which can be explained in terms of the sampling strategy. As described in section 3.4.1, the sampling strategy used in the experiment was the internal recording with averaging time of 10 seconds, dwelling for 30 seconds at each sampling point (giving as a result 3 mean velocities). The sampling time used during the experiment was insufficient to fully characterize the turbulent velocities. Large standard

error values indicate that the turbulent conditions were prevalent in the cross section and larger dwelling times would be needed to fully characterize the turbulence. In future studies concerned with velocity distributions, it is suggested that sampling incorporate a real time continuous sampling strategy with a minimum sampling interval of 3 seconds (equipment specification), and dwelling time of at least 60 seconds ($dwelling\ time\,(s)/3\,(s) = number\ of\ samples$); or an adaptive sampling technique (the probe stays at the specified point until the standard error reported is lower than the user-defined threshold. See (Singh et al., 2007).

For the high variability near the water surface, wind effects can play a role. For this reason, it is suggested that a weather station be installed next to the experimental site in order to compare the wind speed and wind direction data against the reported velocity values close to the water surface. Also, a "settling" time of 5 seconds is suggested before collecting samples once the node is located at the top sampling point of the vertical profile.

In spite of the fact that during the experiment there were no sampling points located below 0.18 of the profile depth $(0.18D)$, it is important to note that for sampling points close to the bed, the sensor manual (Sontek) explains that sources of error near boundaries can be present when the sampling volume of the sensor is actually located in the boundary and not in the water and suggests special care when a moving bed is present. As a general rule, a minimum clearance of 0.2 meters from the bed has to be maintained, thus accounting for the distance from the sensor's probe tip to the sampling volume (0.1 m), and possible changes in the bed (although this value can be larger depending on the dynamics of the river bed). The NIMS RD system is currently under improvement in order to guarantee that the node is able to accurately locate the probe as close to the boundary as the sensor constraints allow.

Even with the high variability present in the measurements, it is possible to distinguish two different zones corresponding to the relatively slow San Joaquin side stream $(0.57 \prec y^* \prec 0.68)$, and the relatively fast Merced side stream $(0.35 \prec y^* \prec 0.54)$--see Figure 4-9.

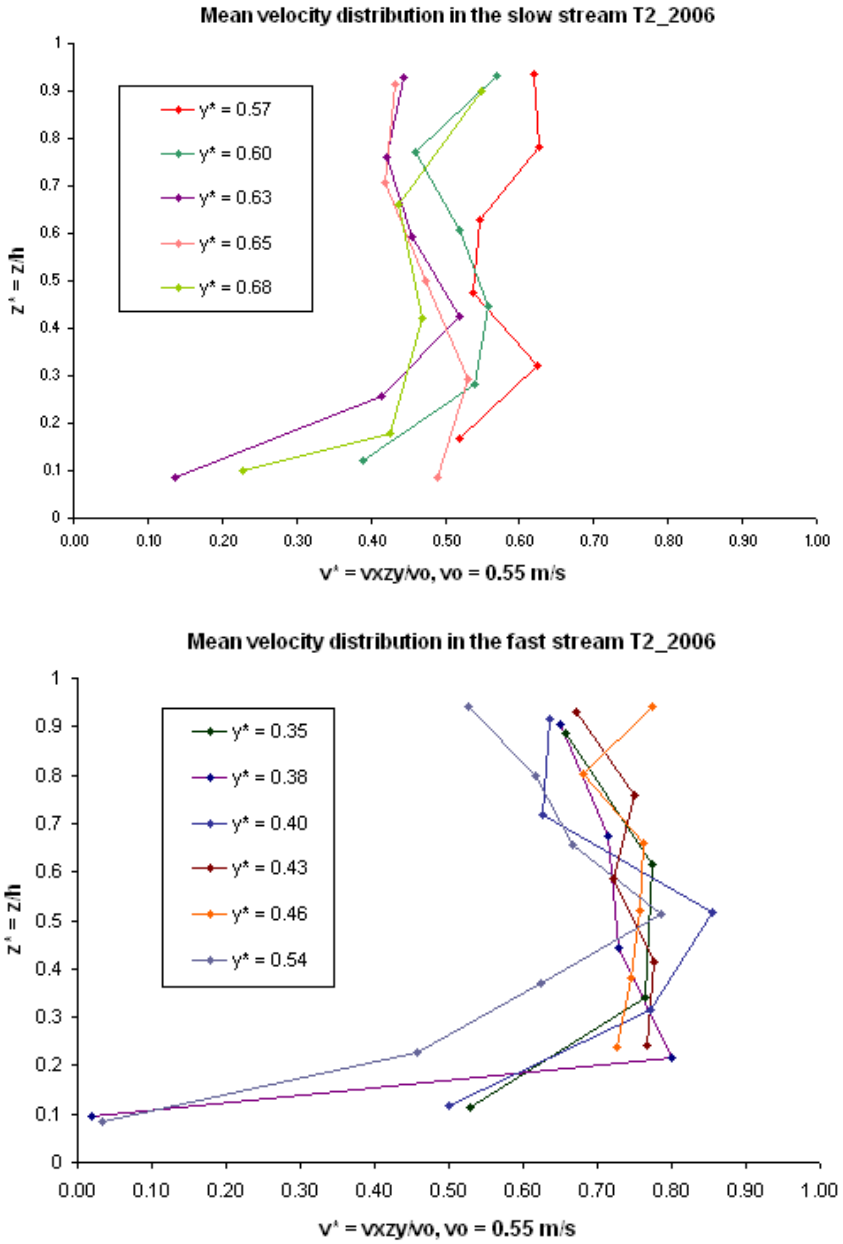

Figure 4-9. Distribution of the mean velocities for Transect 2. Trend towards similarity. Slow stream (top). Fast stream (bottom).

4.4 Analysis of Transect 1 (2007)

4.4.1 General flow description

Transect 1 (2007) has a cross sectional area (A) of 61.71 m^2, a maximum water depth (D) of 2.10 m, a width (b) of 40 m, and an aspect ratio ($\alpha = b/D$) of 19.04. Using the same analysis as was presented in section 4.3.1, Table 4-1 summarizes the flow characteristics for each one of the raster scans. Again, subcritical-turbulent flow conditions were maintained during all of the experiments.

Table 4-1. Flow description for the raster scans on Transect 1 (2007)[‡]

Run	Average Velocity (m/s)	Average Temperature (Deg C)	Kinematic Viscosity (m^2/s)	Re_x	Fr
1	0.18	24.8	9.015E-7	2.52E5	0.040
2	0.18	26.5	8.734E-7	2.60E5	0.040
4	0.19	26.3	8.778E-7	2.73E5	0.042
5	0.18	26.3	8.778E-7	2.58E5	0.040
17	0.17	25.8	8.845E-7	2.42E5	0.037
26	0.18	28.9	8.405E-7	2.70E5	0.040
27	0.15	24.9	8.997E-7	2.10E5	0.033

4.4.2 Descriptive analysis of the velocity profile

For each of the runs, analysis is developed spanwise from $y = 6\,m$ to $y = 34\,m$ $(0.15 \le y^* \le 0.85)$. As described for Transect 2, velocity components correspond to a coordinate system transformation from ENU to xyz-cross section system; normalizations were performed for the depth $(z^* = z/h)$ and velocity magnitudes $(v^* = vxyz/v_0)$, where v_0 corresponds to a maximum value of $0.3\,m/s$; outliers were filtered from the data sets,

[‡] Runs 4 and 5 did not include a multiparameter during the experiment. The temperature value corresponds to the averaged value for the other runs.

and application of the t-test for the 95% confidence level over the sampled velocities at each sampling point was done.

Figure 4-10 presents the distribution of the normalized velocities ($v^* = vxyz / v_o,\ v_o = 0.3\,m/s$) along the normalized depth ($z^* = z/h$). The smaller confidence intervals indicate a better estimate of the mean velocity distribution due to the improvement in the sampling strategy. Comparison with Figure 4-10(c) (run 05) suggests that that larger averaging times significantly reduce the confidence intervals of the velocity profile. The largest variability exists in Figure 4-10(b) (run 02), corresponding to a 30-sec averaging interval.

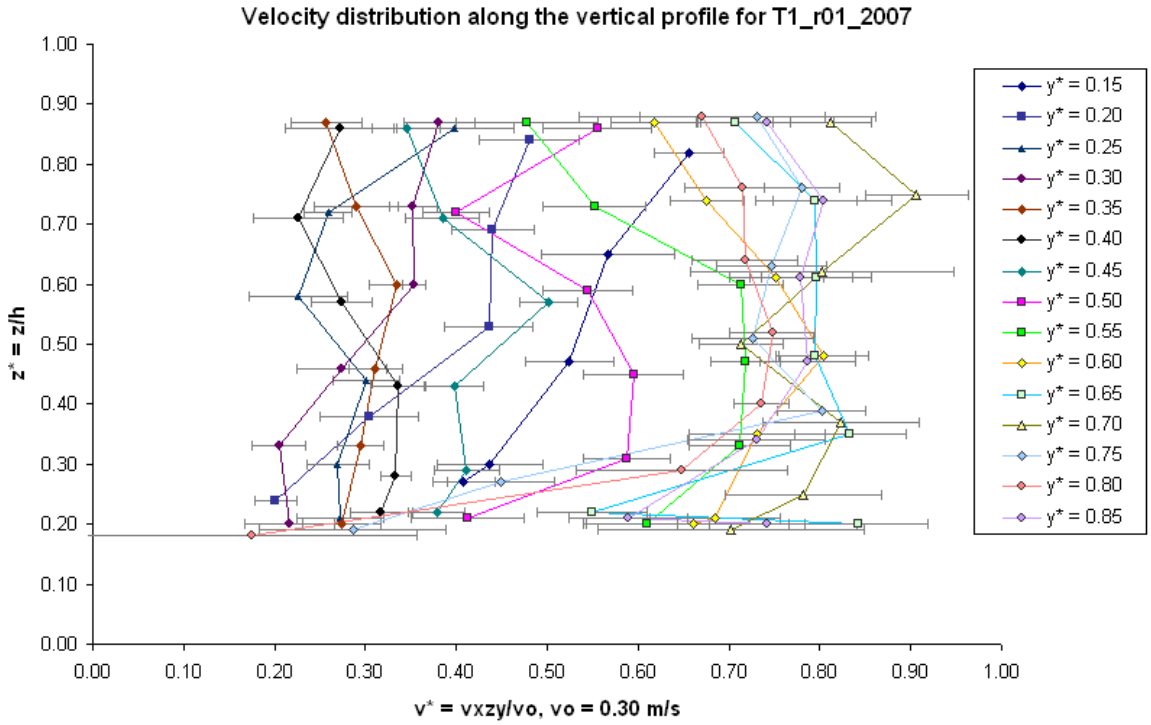

a. Run 01. 60-sec averaging time.

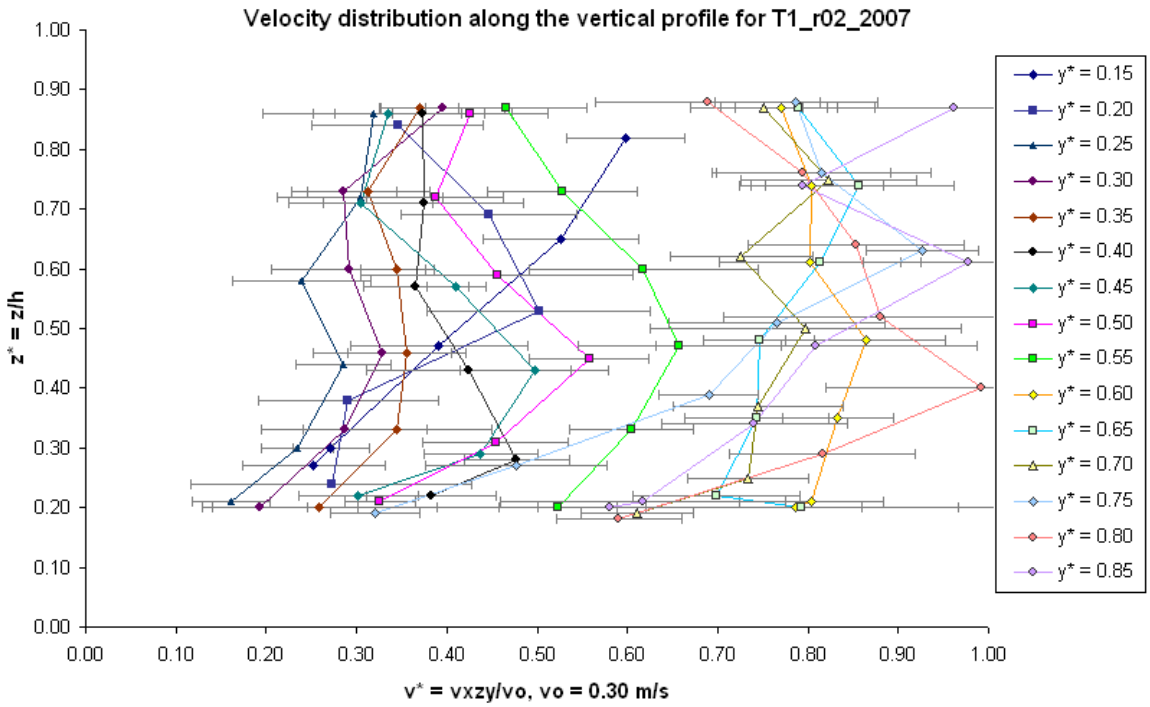

b. Run 02. 30-sec averaging time

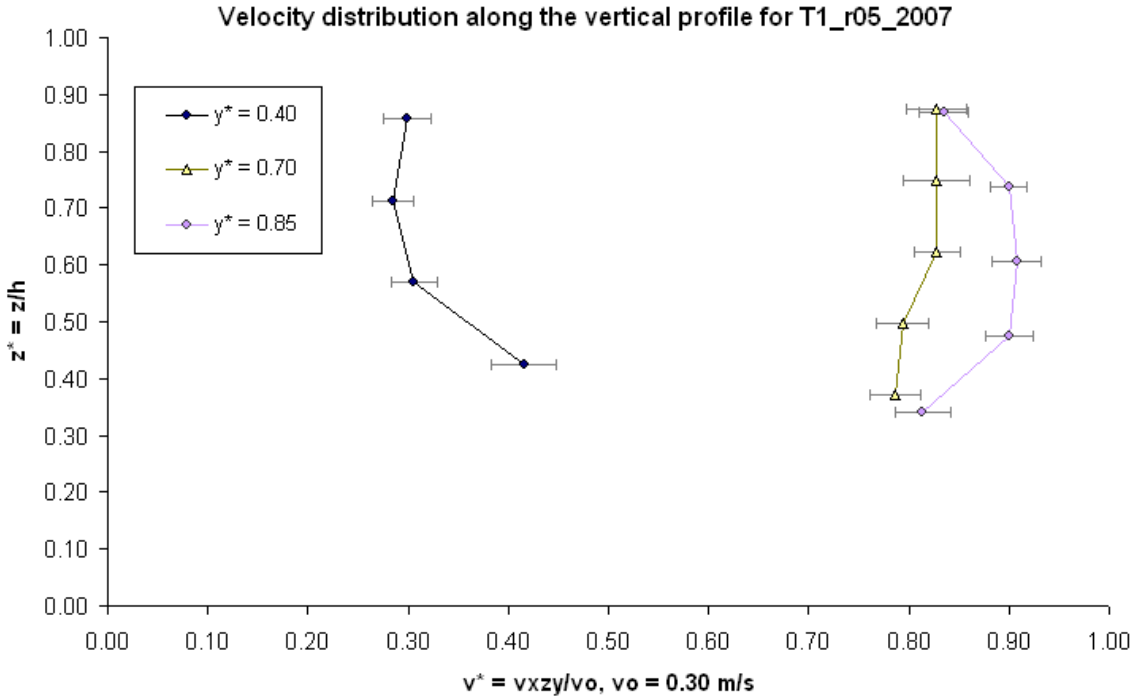

c. Run 05. 300-sec averaging time

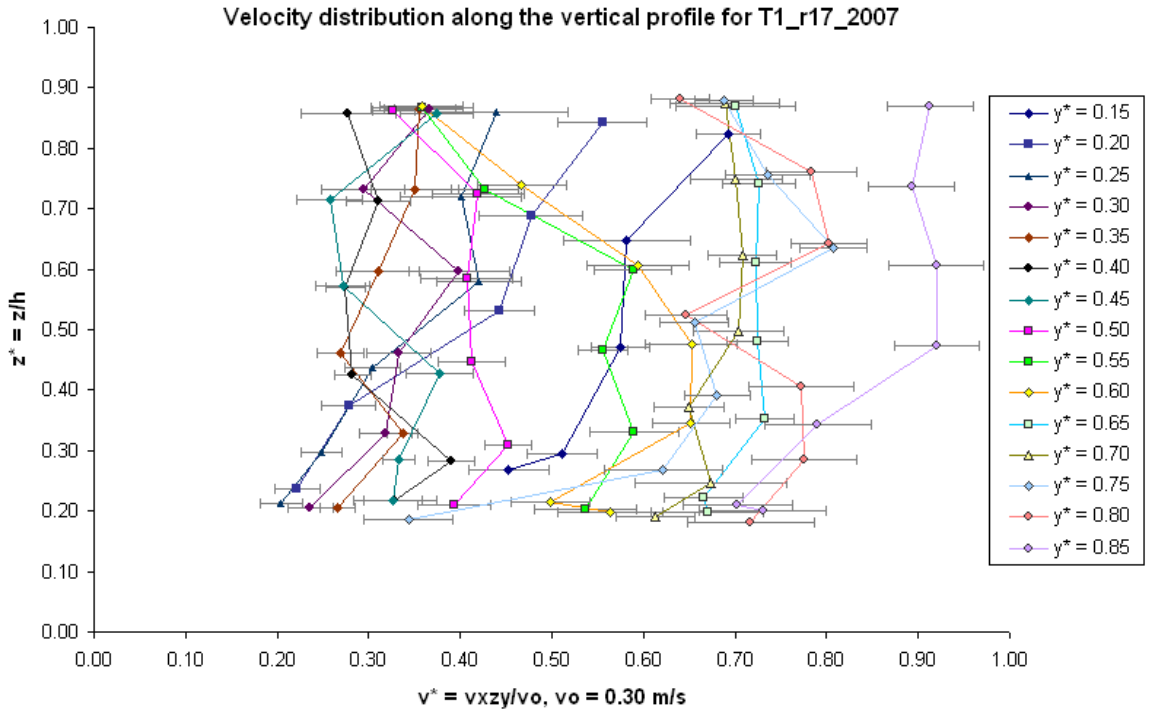

d. Run 17. 60-sec averaging time

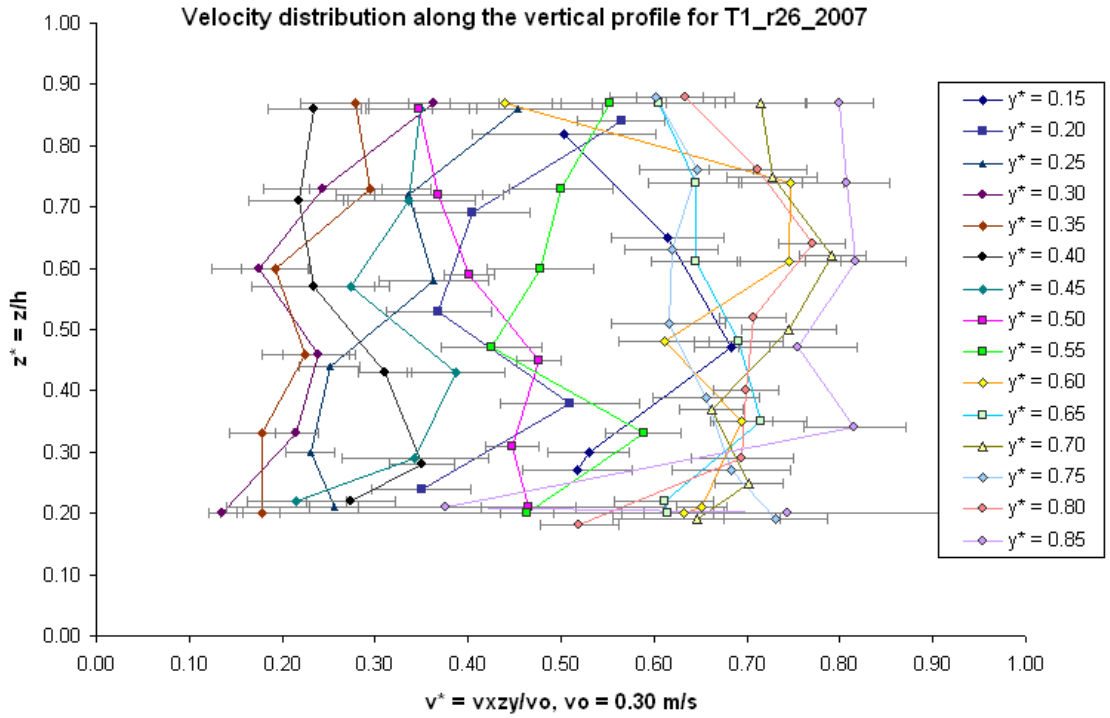

e. Run 26. 60-sec averaging time

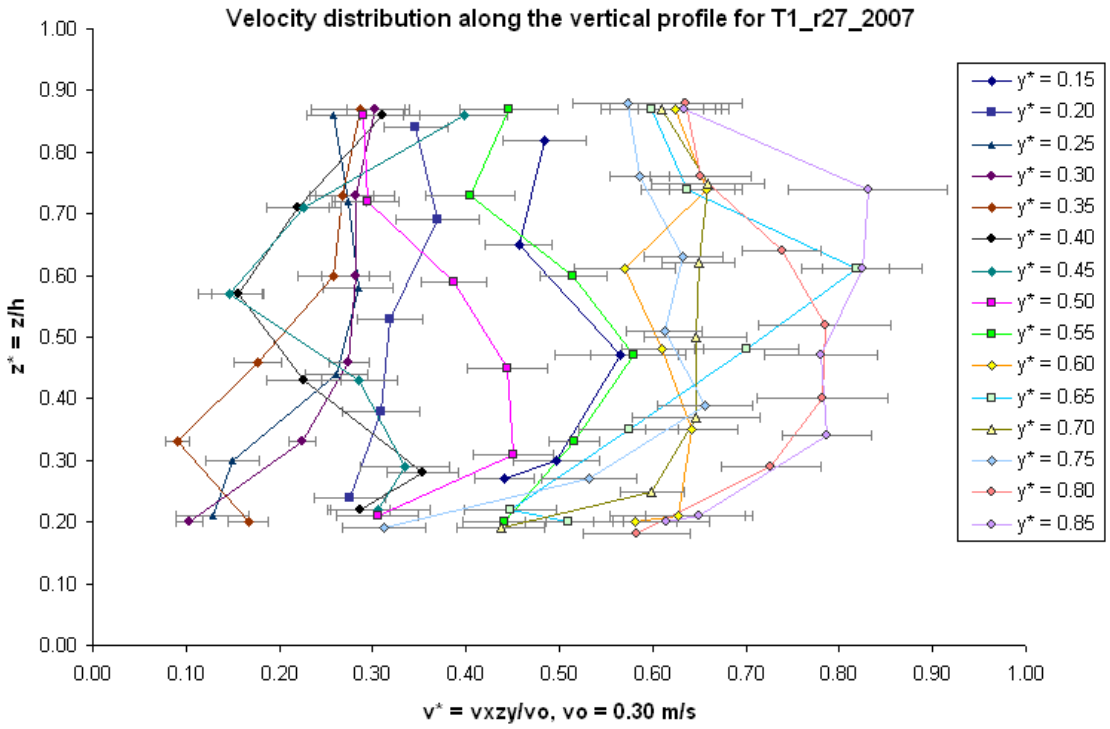

f. Run 27. 60-sec averaging time.

Figure 4-10. Vertical velocity profile in Transect 1. y*= 0 at the Merced side bank and y*=1 at the San Joaquin side bank.

All of the runs allow one to distinguish between the relatively fast stream $(0.60 \prec y^* \prec 0.85)$, the relatively slow stream $(0.25 \prec y^* \prec 0.50)$, and the mixing layer $(0.50 \prec y^* \prec 0.60)$, and the presence of a secondary current on the Merced bank side $(y^* \prec 0.20)$.

4.5 Analysis of the vertical profile of the velocity. Logarithmic profile.

Using the descriptive velocity analysis as a foundation, it is clear that the fitting process for the vertical profile needs to be defined according to the outer variables of the velocity profile (maximum velocity and δ) in the region $0.2 \le z/\delta \le 1.0$ (since there are no actual measurements in the $z/\delta \le 0.2$ to fit the inner region). The logarithmic fitting equation has the form:

$$\frac{u_{\max}-u}{u_{\max}} = -\frac{1}{\alpha\kappa}\ln\left(\frac{z}{\delta}\right)+C\,, \qquad \textbf{(4-14)}$$

where, as mentioned above, $u_{\max}$ is the maximum velocity within the profile, u is the measured (averaged) velocity at each z point, δ is the distance from a reference level at the bottom to the point at which the velocity is maximum within the profile, and κ is the von Kármán constant (0.41). The parameters α and C are empirical fitting parameters. Table 4-2 and Figure 4-11 present the results obtained for Transects 2 and 1.

Table 4-2. Parameters obtained for the fitting process to a logarithmic profile

Transect / Run	α	$A=\frac{1}{\alpha*\kappa}$	C	R^2
T2	9.2527	0.2636	0.0014	0.4219
T1 / Run 01	15.4957	0.1574	0.0537	0.2233
T1 / Run 02	9.6251	0.2534	0.0525	0.4165
T1 / Run 17	9.3953	0.2596	0.0092	0.5318
T1 / Run 26	9.8546	0.2475	0.0600	0.3926
T1 / Run 27	10.1204	0.2410	0.0333	0.3682

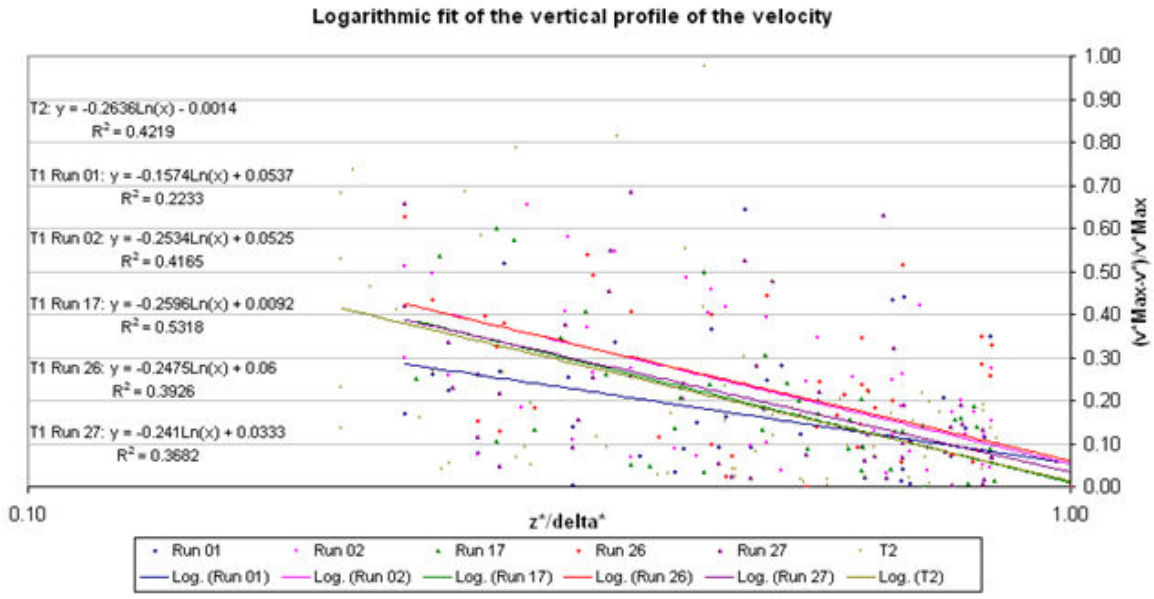

Figure 4-11. Logarithmic fit of the vertical profile of the velocity for the outer region.

With the exception of run 01, and for the range under consideration $(0.2 \le z/\delta \le 1.0)$, the measured data presents a clear trend towards similarity and this would be expected to improve for larger dwelling times.

4.6 Analysis of the transverse depth-averaged velocity profile

For Transect 2 (2006), Figure 4-12 presents the depth-averaged transverse velocity profile. Although a trend towards the theoretical profile can be identified, the presence of various spikes along the profile reflects the necessity of larger averaging times. For the time of the experiment, the FFB station reported an inflow of $8.34\, m^3/s$ while the MST station reported $24.75\, m^3/s$. In this context, and assuming that there are not significant gains or losses between the gauging stations and the confluence, it is possible to confirm that the fast stream is located by the Merced side at 0.42 and the slow stream is located by the San Joaquin side at 0.65. Two important observations can be made from this profile. First, the assumption of uniform velocity in the ambient streams $(U_1 : Merced, U_2 : San\ Joaquin)$ is not accomplished. This situation can be explained in terms of the irregularity of the river cross section and the non-uniformity of the shear stresses at the wall. Second, a smaller width of the mixing layer (δ) is distinguished, compared with Transect 1 (2007). According to (Booij & Tukker, 2001), the greatest mixing layer widths and development lengths correspond to cases in which there are larger velocity differences between the two confluent rivers. Larger velocity differences exist between the confluent rivers in Transect 2 (2006). In support of this second observation it is also important to notice that Transect 2 (2006) is located 135 m downstream of the confluence point (earlier development length of the mixing layer), while Transect 1 (2007) is located 290 m downstream.

For Transect 1 (2007), Figure 4-13 presents the normalized depth-averaged transverse velocity profiles. Seven profiles are displayed (see Table 3-1 and Table 3-2 for reference information for each profile). The first observation to be taken from the figure pertains to

the presence of the relatively fast stream on the San Joaquin side. Although for all of the cases the inflow is slightly higher for the Merced River station (assuming no significant gains or losses until reaching the confluence), the junction angle and the bed morphology (dominant factor for the very low flow conditions), influenced the formation of a fast stream downstream of the confluence towards the San Joaquin Side.

The transverse depth-averaged velocity profile is well reproduced for all the cases on the slow stream side (below normalized distance 0.60) except for the case of run 02 (30-second sampling time) which follows the general trend, but presents a less well-approximated shape. After a normalized distance of 0.60, there appears to be more variation in the depth-averaged values, suggesting the necessity for larger sampling times. Runs 04 and 05 serve as more important references since they have sampling times of 300 s (with the inconvenience that they do not reflect averaged velocities for a raster experiment). Run 04 reports averaged velocities for 5 points located 0.75 m below the water surface at the normalized distances (0.15, 0.35, 0.55, 0.75, and 0.95). Run 05 reports averaged velocities for three vertical profiles located at the normalized distances (0.4, 0.7, and 0.85). It can be seen that for the fast stream side the two profiles present a very similar behavior while the other five profiles (runs 01, 02, 17, 26, and 27) present a different trend.

A last observation can be made in terms of the development of the mixing layer which is very well defined between normalized width 0.35 and 0.70. Due to the smaller velocity differences and the farther downstream location of the transect $(290m)$, it is possible to say that the development length of the mixing layer has been reached (contrary to Transect 2's mixing layer width which appears to be in early formation).

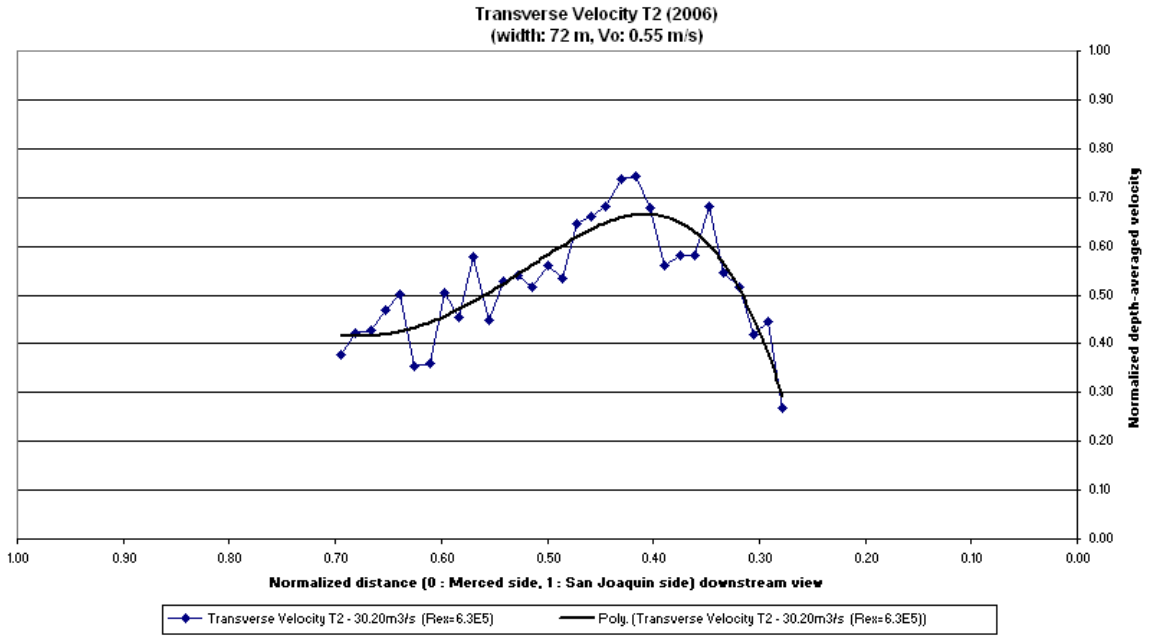

Figure 4-12. Normalized depth-averaged transverse velocity profile Transect 2 (2006)

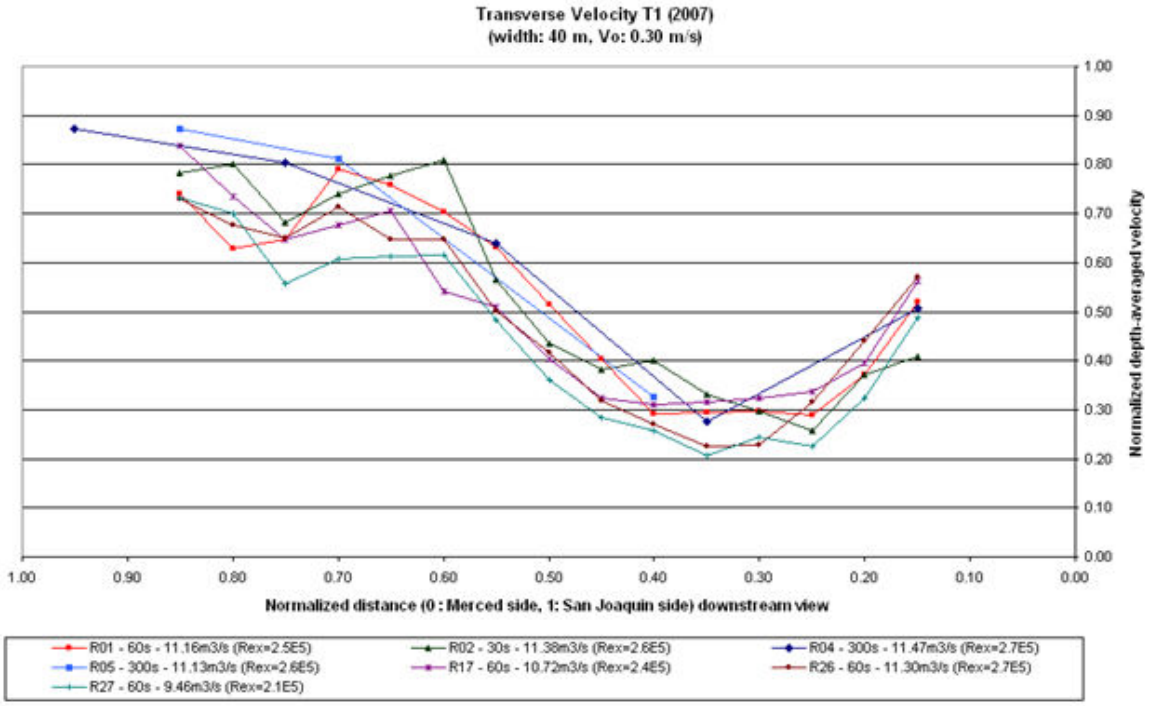

Figure 4-13. Normalized depth-averaged transverse velocity profile Transect 1 (2007)

5 Conclusions and Recommendations

NIMS RD facilitates the detailed characterization of a river transect in terms of flow and water quality parameters. The case of the confluence zone in the San Joaquin River provides an opportunity to consider important questions such as those pertaining to the correlation among water quality parameters on a daily, monthly, or seasonal basis; the mixing processes between two rivers (validation of the current models), and the calculation of flow and mass balances in a river reach oriented to the understanding of non-point source pollution or the identification of groundwater-surface water interactions, among others. When flow and mass balances are the interest, the velocity distribution is the main variable in the system.

A descriptive analysis of the vertical velocity profiles permitted the study of the validity of the sampling strategy employed. Comparison of the confidence intervals of the averaged velocities obtained with a t-test for 30, 60, and 300-second dwelling times reflect their importance in the characterization of the turbulence structures. The 300-second dwelling time presented the smallest confidence intervals and was able to represent a better approximation of the shape of the typical velocity profile when compared to theoretical profiles. Also, for all the data sets, the descriptive analysis allowed differentiating between the three different zones within the cross section downstream of a confluence: the slow stream, the fast stream, and the mixing layer.

The proposed sampling results strongly point to the need for an adaptive sampling strategy aimed at achieving a pre-defined precision level, instead of fixed dwelling times for all the sampling points. For the measurements close to the river bed, it is suggested (for the ADV geometry used here) that the velocimeter be deployed no less than 0.20 meters from the river bed to account for the 0.10 m length from the sensor tip to the sample volume and for the dynamics of a moving bed. For measurements done in the top of the vertical profile, a “resting” time of 5 seconds is suggested in order to bring the sensor to equilibrium. In addition, the use of a weather station is expected to help to

validate the measured velocities close to the water surface with supplemental information of wind speed and direction.

Based on the log-wake law, a logarithmic fit was found to apply reasonably well for all of the analyzed vertical velocity profiles except one (run 01 Transect 1). The fitting process was performed for velocities located within the $0.2 \le z/\delta \le 1.0$ zone since no data for the inner region of the profile was collected during the experiments. The characteristic length and velocity scales for the outer region were used allowing to obtain a fitting equation with the form: $\frac{u_{\max} - u}{u_{\max}} = -\frac{1}{\alpha\kappa}\ln\left(\frac{z}{\delta}\right) + C$.

The analysis of the transverse depth-averaged velocity profile was expanded in order to verify whether or not the data collected with the NIMS RD system was capable of characterizing the mixing layer present downstream of the confluence zone. For Transect 2 (2006), although a trend toward the theory can be identified, the presence of various spikes along the profile reflects the necessity of larger averaging times. Also, in terms of the analysis of the mixing layer development, due to its closer proximity to the confluence of the two rivers, a small width is observed. Thus, its development is in an early stage due to the large mean velocity difference between the inflow streams.

The data sets analyzed for Transect 1 (2007) represent a much better approximation to the theory. The advantage of larger dwelling times can be appreciated after comparison of the transverse profiles for 30, 60, and 300-sec, and with the measurements done for Transect 2. The profiles clearly differentiate the fast stream, the slow stream, and the mixing layer and support the proposition of adaptive sampling since the smoothness observed in the profiles, both in the slow stream and mixing layer zones, is reduced when reaching the fast stream side of the cross-section.

References

APHA. (1999). 2510 conductivity. In A. E. Greenberg (Ed.), *Standard methods for the examination of water and wastewater* (pp. 2-44-2-48). Washington, D.C.: American Public Health Association.

Best, J. L. (1987). Flow dynamics at river channel confluences: Implications for sediment transport and bed morphology. *Recent Developments in Fluvial Sedimentology: Contributions from the Third International Fluvial Sedimentology Conference,* Tulsa, Oklahoma, USA. *, 39* 27-35.

Biron, P. M., Ramamurthy, A. S., & Han, S. (2004). Three-dimensional numerical modeling of mixing at river confluences. *Journal of Hydraulic Engineering, 130*(3), 243-253.

Booij, R., & Tukker, J. (2001). Integral model of shallow mixing layers. *Journal of Hydraulic Research, 39*(2), 169-179.

Brown, L. L., Panshin, S. Y., Kratzer, C. R., Zamora, C., & Gronberg, J. M. (2004). *Occurrence, distribution, instantaneous loads, and yields of dissolved pesticides in the San Joaquin River basin, California, during summer conditions, 1994 and 2001* (Scientific Investigation Report No. sir2004-5083). Sacramento, California: U. S. Geological Survey. Retrieved June, 2006.

California Department of Water Resources. (2007). *California data exchange center.* Retrieved May/2007.

De Serres, B., Roy, A. G., Biron, P. M., & Best, J. L. (1999). Three-dimensional structure of flow at a confluence of river channels with discordant beds. *Geomorphology, 26*, 313-335. Retrieved June, 2006.

Department of Water Resources, Bay-Delta Office. (2002). *CALSIM water resources simulation model*. California. Retrieved December, 2005.

Dubrovsky, N. M., Kratzer, C. R., Brown, L. L., Gronberg, J. M., & Burow, K. R. (1998). *Water quality in the San Joaquin-=Tulare basins, California, 1992-1995* (Circular No. circ1159). California: U. S. Geological Survey. Retrieved June, 2006.

Gonzalez, J. A., Merching, C. S., & Oberg, K. A. (1996). Analysis of open-channel velocity measurements collected with an acoustic Doppler current profiler. Paper presented at the *1st International Conference on new/emerging Concepts for Rivers,* Chicago, Illinois, USA. 1-8. Retrieved January 25., 2007.

Gronberg, J. M., Dubrovsky, N. M., Kratzer, C. R., Domagalski, J. L., Brown, L. L., & Burow, K. R. (1998). *Environmental setting of the san Joaquin-Tulare basins, California* (Water-Resources Investigations Report No. wrir97-4205). Sacramento, California: U. S. Geological Survey. Retrieved June, 2006.

HACH Environmental. *Hydrolab DS5X, DS5, and MS5 water quality multiprobes user manual.* Retrieved March/13, 2007.

Harmon, T. C., Ambrose, R. F., Gilbert, R. M., Fisher, J. C., Stealey, M., & Kaiser, W. J. (2007). High-resolution river hydraulic and water quality characterization using rapidly deployable networked infomechanical systems (NIMS RD). *Environmental Engineering Science, 24*(2), 151-159. doi:10.1089/ees.2006.0033

Kironoto, B. A., & Graf, W. H. (1995). Turbulence characteristics in rough non-uniform open-channel flow. *Proceedings of the Institution of Civil Engineers, 112*, 336-348.

Kratzer, C. R., & Shelton, J. L. (1998). *Water quality assessment of the San Joaquin-Tulare basins, California: Analysis of available data on nutrients and suspended sediment in surface water, 1972-1990* (Professional Paper No. pp1587). California: U. S. Geological Survey. Retrieved June, 2006.

Miller, R. L., Bradford, W. L., & Peters, N. E. (1988). *Specific conductance: Theoretical considerations and application to analytical quality control*. Washington, D.C.: U.S. G.P.O.

Nezu, I., & Nakagawa, H. (1993). *Turbulence in open-channel flows*. Netherlands: A.A. Balkema, Rotterdam.

Nezu, I., & Rodi, W. (1985). Experimental study on secondary currents in open channel flow. *21st Congress of IAHR,* Melbourne, Australia. *, 2* 115-119.

Rhoads, B. L., & Sukhodolov, A. N. (2004). Spatial and temporal structure of shear layer turbulence at a stream confluence. *Water Resources Research, 40*, 1-13. Retrieved March, 2007.

Singh, A., Batalin, M. A., Chen, V., Stealey, M., Jordan, B., Fisher, J. C., et al. (2007). Autonomous robotic sensing experiments at San Joaquin River. Paper presented at the *Robotics and Automation, 2007 IEEE International Conference on,* 4987-4993.

SonTek. (2007). *Argonaut-ADV and FlowTracker principles of operation.* Retrieved March/01, 2007.

Sukhodolov, A. N., & Rhoads, B. L. (2001). Field investigation of three-dimensional flow structure at stream confluences. *Water Resources Research, 37*(9), 2411-2424. Retrieved March, 2007.

Tachie, M. F., & Bergstrom, D. J. (2000). Rough wall turbulent boundary layers in shallow open channel flow. *journal of Fluids Engineering, 122*, 533-541.

White, F. M. (2006). Incompressible turbulent mean flow. *Viscous fluid flow* (3rd ed., pp. 398-504). New York, USA: McGraw-Hill.